Development of an On-Line Entrainment Measurement Device for a Bubbling Fluidized Bed

Maria Aletta Müller

UNIVERSITEIT VAN PRETORIA
UNIVERSITY OF PRETORIA
YUNIBESITHI YA PRETORIA

Development of an On-Line Entrainment Measurement Device for a Bubbling Fluidized Bed

by

Maria Aletta Müller

A thesis submitted in fulfillment
of the requirements for the subject CVD 800

Masters of Engineering (Chemical Engineering)

in the

Chemical Engineering
Faculty of Engineering, the Built Environment and Information Technology

University of Pretoria
Pretoria

28 September 2012

Development of an On-Line Entrainment Measurement Device for a Bubbling Fluidized Bed

Author: Maria Aletta Müller
Supervisor: W. Nicol
Department: Department of Chemical Engineering
University of Pretoria
Degree: Masters of Engineering (Chemical Engineering)

Synopsis

A selective combination of the principles of a thermal mass flow meter and constant temperature anemometry was used to develop a solid mass flow meter that improves significantly on the flow meter developed by De Vos *et al* (2010). The flow meter has a measurement plate that is kept at a constant temperature. Due to conductive heat transfer between the entrained solids and the measurement plate, additional power is needed to maintain the plate at this setpoint temperature value. This additional power was correlated against the average solids flow rate.

The calibration curve shows a linear relationship between the power measurement and the entrainment flux for entrainment fluxes between 3.4×10^{-4} kg/(m^2.s) and 7.5×10^{-3} kg/(m^2.s). Deviation from a linear response at lower entrainment fluxes may be caused by a longer residence time of fine particles on the measurement plate due to lower shear forces. At higher entrainment fluxes the power measurements were unreliable due to poor temperature control. The turndown ratio of the linear section of the calibration curve is approximately 3 times that of the linear part of the calibration curve of the flow meter developed by De Vos *et al* (2010). Even further improvement is possible with better temperature control.

In a case study to test the applicability of the flow meter to measure changes in entrainment rate associated with hydrodynamic properties other than a change in gas superficial velocity, small amounts of ethanol were dosed to the inlet air. The continuously measured entrainment rate increased at lower ethanol dosing rates but decreased as the dosing rate of ethanol was increased. The increase in entrainment rate may be explained by a reduction in static electricity in the bed, while the decrease at higher dosing rates may be as a result of increased powder cohesivity.

KEYWORDS: solid mass flow meter, entrainment rate, bubbling fluidized bed

Contents

List of figures

List of tables

Acknowledgements

I would like to express my gratitude to:

- Necsa Department of Nuclear Engineering, under the supervision of Mr. JD Adendorff for providing the laboratory space in order to conduct the investigation. Also for providing the necessary equipment and materials for the investigation.

- Mr. D Cilliers, Colibri Technology, for setting up and providing the necessary electronic equipment.

- Prof. W Nicol and Mrs. EL Du Toit, Department of Chemical Engineering, University of Pretoria, for guidance and expert advice throughout the investigation.

Nomenclature

Ar	Archimedes number
d_p	Particle diameter (m)
E	Entrainment flux (kg/(m^2.s))
FET	Field Effect Transistor
g	Gravitational acceleration (m/s^2)
Necsa	Nuclear Energy Corporation of South Africa
NPT	National Pipe Thread
P	Power (Watt)
PI	Proportional - Integral
PVC	Poly(Vinyl Chloride)
PWM	Pulse Width Modulation
$(Re)_{mf}$	Particle Reynold's number at minimum fluidization
T_a	Ambient temperature in dipleg (° C)
T_1	Temperature of lower part of brass plate (° C)
T_2	Temperature of upper part of brass plate (° C)
TDH	Transport Disengagement Height (m)
u	Superficial fluid velocity (m/s)
u_c	Characteristic velocity when bubbles are at their maximum size (m/s)
u_k	Velocity corresponding to a steady state in the standard deviation of the pressure fluctuation curve (m/s)
u_{mb}	Minimum bubbling velocity (m/s)
u_{mf}	Minimum fluidization velocity (m/s)
U	Superficial gas velocity (m/s)
USB	Universal Serial Bus

Greek

ε_{mf}	Porosity of the bed at minimum fluidization
$\emptyset$	Particle shape factor
ρ_f	Density of the fluid (kg/m^3)
ρ_p	Particle density (kg/m^3)
μ	Viscosity of the fluid (kg/m.s)

1. Introduction

Gas-solid fluidized bed reactors are used for various reasons and in a wide variety of industries. Most commercial applications of fluidized beds are concerned with catalytic reactions (e.g. Fisher-Tropsch synthesis and catalytic cracking of hydrocarbons) and gas-solid reactions such as gasification processes which are used to convert coal, biomass or waste material into synthesis gas (Parr, 2012).

In fluidized beds, entrainment is the total amount of solids carried out of the bed (Almendros-Ibáñez *et al*, 2009). The entrainment rate increases with the gas velocity to the power of 2 to 4, therefore entrainment is much lower for bubbling fluidized beds than for beds operated in the fast fluidization regime (Yang, 2003: 118). Most fluidized beds employ a system of returning the entrained solids: for low superficial velocities or bubbling beds internal cyclones are used, while external cyclones are typically employed for fast fluidization systems (Kunii & Levenspiel, 1990).

Knowledge of the entrainment rate is needed to comply with pollution control regulations and to maintain fluidization quality (Briens *et al*, 1992). The performance and design of separation equipment such as cyclones and bag filters are affected by the entrainment rate (Fung & Hamdullahpur, 1993). Entrainment has an effect on the selectivity of reactions and the contact efficiency between the gas and solids in a gas-solid fluidized reactor (Hatano & Ishida, 1983). It is therefore important to continuously measure the entrainment rate even for processes with low entrainment.

In practice fluidization is almost entirely based on empirical correlations in terms of the design and scale-up (Yang, 2003: 53) and specifically so in the measurement of the entrainment rate (Choi *et al*, 1999). Correlations have been proposed in order to determine the entrainment rate, but there exist considerable

discrepancy between the results obtained by different authors in literature (Do, Grace & Clift, 1972); sometimes the difference in their findings is more than an order of magnitude (Kunii & Levenspiel, 1991: 168). It is clear that the empirical correlations available for estimating entrainment rate can only be used if the particle properties and operating conditions are the same as the conditions which were used to develop the correlations.

A novel on-line total entrainment measurement device, specifically for use in bubbling fluidized beds with relatively low entrainment rates, was developed by De Vos and co-workers (2010). The measurement device was based on the principles of a thermal mass flow meter. The change in temperature of the measurement device due to conductive heat transfer between the entrained solids and the device was measured indirectly by making use of a thermistor. One of the main shortcomings of this device is the nonlinearity of the calibration curve at high entrainment rates which implies a loss in sensitivity of the measurement device. The loss in sensitivity to changes in the inferred temperature is due to a decrease in the temperature gradient available for heat transfer as the amount of cooling of the measurement device increases (Nicol, 2011).

The purpose of this investigation was to develop an on-line entrainment measurement device which is an improvement of the device developed by De Vos and co-workers (2010). The measurement device must conform to the following: temperature must be measured directly to create a faster response; the temperature must be controlled in order to use a fixed temperature gradient; and the device must be able to monitor the entrainment when an operating variable is changed e.g. gas velocity or the electrostatic condition of the bed.

Selective literature on fluidization and entrainment rate and its measurement are given in Section 2. In Section 3 the details of the mass flow meter developed in this work, as well as of the fluidized bed where it was tested, are given.

Section 4 explains how the data from the flow meter was handled in order to construct the calibration curve. It includes discussion on all the possible factors that can influence the measurement and explains how they were measured and or treated when the calibration curve was constructed. Section 4 also includes a comparison between this flow meter and the one developed by De Vos and co-workers (2010). In order to test the applicability of the device to measure changes in entrainment rate due to hydrodynamic effects other than a change in gas superficial velocity, small amounts of ethanol were dosed to the inlet air in a case study that is briefly discussed in Section 5.

2. Theory

In Sections 2.1.1 to 2.1.3 gas-solid fluidization is discussed as well as the different fluidization regimes. In Section 2.2 entrainment and the factors affecting entrainment are discussed together with the different methods used to measure entrainment rate.

2.1 Gas-solid fluidization

2.1.1 Classification of powders

Depending on the density of the solids and the fluid used during fluidization and the mean particle size of the particles; solids are divided into four groups. Each group represents a particular behaviour of the solids when fluidized. This classification of solids is known as the Geldart classification. The behaviour exhibited by the solids in the different groups is given in Table 1 (Yang, 2003: 54).

Table 1: Behaviour of solids when fluidized according to the Geldart classification

Group	Solid behaviour when fluidized
A	The bed of solids first expands after the gas velocity is reached at which the solids are completely fluidized. Then with a further increase in gas velocity gas bubbles appear.
B	When the gas velocity is reached at which the solids are completely fluidized, the first gas bubbles appear.
C	Very difficult to fluidize solids, since the particles are cohesive.
D	Give rise to stable spouted beds.

At ambient conditions Figure 1 can be used to determine in which group the solids under investigation are classified when the fluid and solid densities (ρ_f and ρ_p respectively) and mean particle diameter (d_p) are known (Yang, 2003: 55).

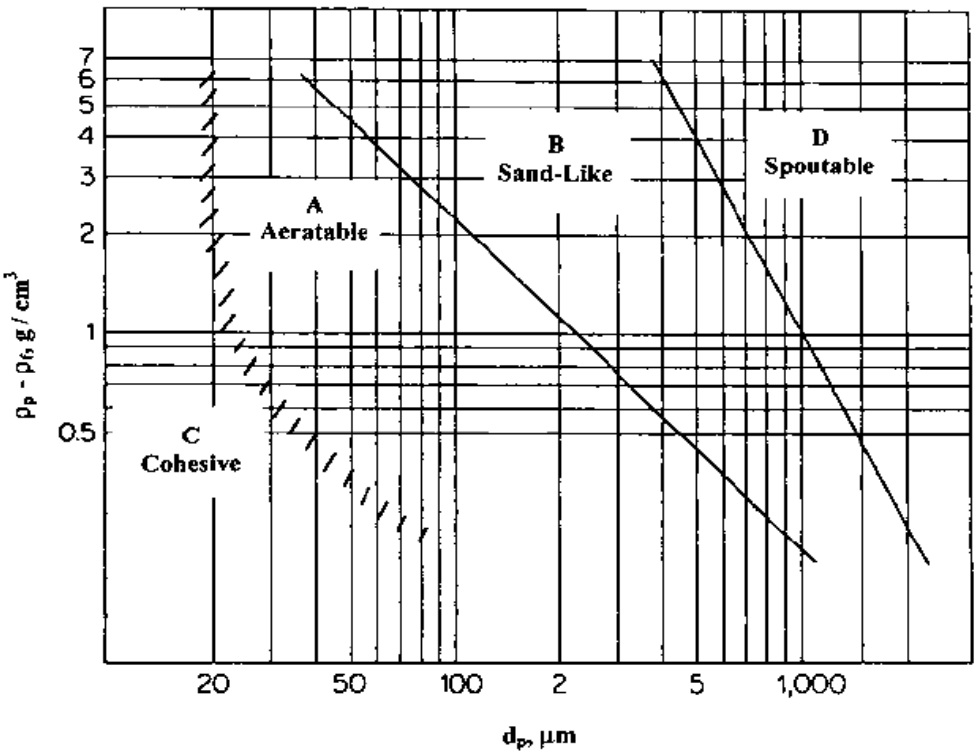

Figure 1: Classification of powders according to Geldart (taken from Yang (2003: 55)).

2.1.2 Fluidization regimes

As the velocity of the gas through the bed of solids is increased, different fluidization regimes can be distinguished. The bed is firstly a fixed packed bed when no gas is passed through the bed. With an increase in gas velocity the gas passes through the particles and no bubbles are observed. As soon as all the particles are completely supported by the gas stream, the gas velocity corresponds to the minimum fluidization velocity. Fluidization in this regime is also known as smooth, particulate or homogeneous fluidization (Yang, 2003: 57-64).

As soon as gas bubbles are observed the gas velocity at that point is known as the minimum bubbling velocity, which is greater than the minimum fluidization velocity for Geldart group A particles and is approximately the same as the minimum fluidization velocity for Geldart group B and group D particles (Yang,

2003: 54). When gas bubbles are present the fluidization is known as heterogeneous, bubbling or aggregative fluidization (Yang, 2003: 57).

Slugging occurs in a small, fluidized bed if the diameter of the bubble reaches a size that is approximately two thirds of the diameter of the column; the large bubbles passes periodically through the entire bed causing large bed pressure drop fluctuations (Yang, 2003: 59).

A further increase in gas velocity above the minimum bubbling velocity causes a turbulent bed if the bed diameter is large compared to the particle diameter. By constructing a plot of the standard deviation of pressure fluctuation and the superficial fluidization velocity, two characteristic velocities are identified namely u_c and u_k. When the bubbles are at their maximum size the first characteristic velocity (u_c) has been reached (corresponding to the largest standard deviation). Increasing the gas velocity above u_c causes the pressure fluctuations to decrease due to the bubbles breaking up into smaller bubbles leading to a steady state in the standard deviation. The velocity corresponding to the eventual steady state in the standard deviation is known as u_k which characterizes the transition between the bubbling regime and the turbulent regime (Yang, 2003: 59).

Increasing the gas velocity above the velocity necessary to maintain the turbulent regime a critical velocity is reached where all of the particles are carried out of the bed. This critical velocity is known as the transport velocity. In order to operate the fluidization reactor continuously the particles carried out of the bed must be recycled. The fluidized bed is now in the fast fluidization regime (Yang, 2003: 61).When the gas velocity is increased high above the transport velocity the fluidization regime known as pneumatic conveying is achieved. In this regime the particle feed is throughout the reactor in dilute phase, therefore no bed surface is present although the solids concentration varies with bed height (Yang, 2003: 59).

In this investigation only operation in the bubbling fluidized regime was considered.

2.1.3 Velocities characterizing the bubbling fluidized regime

Equation 1 can be used to determine the minimum fluidization velocity. It is based on the Ergun equation and the fact that the pressure drop at minimum fluidization is equal to the weight of the particles in the bed (Yang, 2003: 63).

In Equation 1 Ar is the Archimedes number given by Equation 2, ε_{mf} is the porosity of the bed at minimum fluidization, $\emptyset$ is the particle shape factor and $(Re)_{mf}$ is the Reynolds' number of the particle at minimum fluidization. The Reynolds' number is given by Equation 3. In Equations 2 to 6 d_p is the diameter of the particle in m, ρ_f is the density of the fluid in kg/m^3, ρ_p is the density of the particle in kg/m^3, g is gravitational acceleration in m/s^2, μ is the viscosity of the fluid in kg/(m.s) and u is the superficial fluid velocity in m/s (Yang, 2003: 25, 50).

$$Ar = 150\frac{(1-\varepsilon_{mf})}{\emptyset^2\epsilon_{mf}^3}(Re)_{mf} + 1.75\frac{1}{\emptyset\varepsilon_{mf}^3}(Re)_{mf}^2 \quad (1)$$

$$Ar = \frac{d_p^3\rho_f(\rho_p-\rho_f)g}{\mu^2} \quad (2)$$

$$Re_p = \frac{d_p u\rho_f}{\mu} \quad (3)$$

If the minimum fluidization velocity (u_{mf} in m/s) is known, the minimum bubbling velocity (u_{mb} in m/s) can be calculated from Equation 4. The ratio given by Equation 4 has been observed to increase the smaller and lighter the particles are (Yang, 2003: 54).

$$\frac{u_{mb}}{u_{mf}} = \frac{(4.125\ x\ 10^4)\mu^{0.9}\rho_f^{0.1}}{(\rho_p-\rho_f)d_p g} \quad (4)$$

A great deal of correlations exists for the calculation of u_c and u_k (Yang, 2003: 60). Equations 5 and 6 were proposed by Horio (1986) (quoted by Yang (2003: 60)) with the Archimedes number given by Equation 2.

$$\frac{d_p \rho_f u_c}{\mu} = 0.936 Ar^{0.472} \tag{5}$$

$$\frac{d_p \rho_f u_k}{\mu} = 1.46 Ar^{0.472} \tag{6}$$

The minimum bubbling velocity and the turbulent velocity (u_c) can be used to determine the extremes of the bubbling fluidized regime.

2.2 Entrainment

The amount of solids which leaves the fluidization reactor with the gas is known as entrainment (Yang, 2003: 113). Fluidization columns are divided into two sections, a dense phase region in the lower part of the column and a dilute phase region in the rest of the column. As the gas velocity is increased the bed surface starts fluctuating until a clear distinction cannot easily be made between the dense phase and the dilute phase. Above the bed surface the solids holdup decreases until an approximate constant concentration is reached. The height of the column measured between the point where the solid concentration is approximately constant and the bed surface is known as the transport disengagement height (TDH) (Yang, 2003: 114).

Only empirical correlations exist to calculate the TDH; one such correlation is given by Equation 7. In Equation 7 U is the superficial gas velocity in m/s (Yang, 2003: 124).

$$TDH = 0.85 U^{1.2} (7.33 - 1.2 log U) \tag{7}$$

The particles enter the freeboard through various mechanisms; some of the proposed mechanisms are:

- that particles are ejected into the freeboard due to bubbles erupting at the surface of the dense phase (Do *et al*, 1972);
- high drag forces at the surface of the dense phase that cause individual particles to be released from the bed surface into the freeboard (Do *et al*, 1972);
- that the particles which are ejected due to bubbles erupting at the bed surface can enter the freeboard due to particle transportation from the wake of a single bubble, the wake of two bubbles which has first been coalescing or from the roof of a single bubble (Yang, 2003: 114).

It should be noted that entrainment is not the rate at which the bubbles through particles into the freeboard, but it is the amount of those solids thrown up into the freeboard that is carried out of the fluidized reactor with the gas. The largest flux of solids that can be carried out of a fluidized reactor (with a gas exit above the TDH) is represented by the saturation carrying capacity of the gas (Kunii & Levenspiel, 1991: 165). The gas is then saturated with solids.

The focus of this investigation is not the mechanisms which cause entrainment, but rather the measurement of the entrainment rate. Section 2.2.7 describes the different methods that were developed to determine the entrainment rate. Some of the factors affecting entrainment are discussed in Sections 2.2.1 to 2.2.6.

2.2.1 Effect of fines in feed on entrainment

The effect of adding very fine powder (Geldart group C powder) to the feed powder of a fluidization column (e.g. Geldart group A powder) resulted in the entrainment rate to decrease compared to no fines added to the feed of the column (Baeyens, Geldart & Wu, 1992). The reasons are that: if a Geldart group A type powder is used with a small amount of cohesive Geldart group C powder the fine particles adhere to the larger particles, therefore acting like larger particles and not like individual small particles; and if a large amount of cohesive

Geldart group C powder is added it could result that the bed behaves cohesively, therefore fewer particles are present and, therefore fewer particles are ejected into the freeboard, leading to less entrainment (Baeyens *et al*, 1992).

According to Han *et al* (2011) there is a sharp increase in the elutriation rate when the operating gas velocity is close the terminal velocity of the particles. Generally the smaller the particles, the higher the elutriation rate, but if the particle size is too low the elutriation rate decreases due to large adhesion forces resulting in the formation of agglomerates (Han *et al*, 2011).

2.2.2 Electrostatic effects

Static electrification is caused by the motion of particles around gas bubbles. The amount of charge generated is dependent on the mean particle size in the bed. The amount of charge is also affected by relative humidity, the relative humidity affect the rate at which charge is dissipated (Boland & Geldart, 1971).

Katz (1957) (quoted by Boland & Geldart (1971)) found that the static charges in the bed can be limited by using air with a high relative humidity, however he experienced agglomeration problems. Earthing the column in an attempt to reduce electrostatic charges was mostly found to be unsuccessful, since most electrostatic charges are caused by particle-particle and particle-gas interactions and not mainly by interactions with the wall of the column (Park, Bi & Grace, 2002) and ionizing the air was also unsuccessful (Boland & Geldart, 1971).

Geldart and Wong (1985) (quoted by Briens *et al* (1992)) found that the flux of entrained particles was less when they used a fluidizing gas with a humidity above 60 % when they investigated non-porous particles. The reason Geldart and Wong (1985) (quoted by Briens *et al* (1992)) provided was that there is an increase in powder cohesivity with relative humidity and that electrostatic forces which varies with humidity were insignificant. Baron *et al* (quoted by Briens *et al* (1992)) found that the entrainment rate increased with an increase in the

humidity of the fluidizing gas. The reason provided for the increase in the entrainment was a decrease in the electrostatic effects. The entrainment experiments were done by fluidizing sand in the bubbling regime.

Electrostatic effects can be regarded as insignificant at high temperatures and only plays a significant role at low ambient temperatures. At relative humidities less than 60 % the quality of fluidization was not affected according to Briens *et al* (1992). An investigation was conducted by Briens *et al* (1992) on the effect of electrostatics on the size distribution of entrained particles by varying the fluidizing gas humidity (humidity kept under 60 %) and they concluded that all particle sizes were affected by electrostatic charges and that the smallest particles in the bed are not the particles that are most easily entrained. Briens and co-workers (1992) explain that it is due to interparticle forces; the small particles have a greater surface-to-volume ratio than larger particles and are therefore more sensitive to electrostatic forces. The smallest particles are adhered to other bed particles and therefore trapped in the bed due to attractive forces created between particles of different charges due to their difference in surface-to-volume ratios. If the charges are neutralised or reduced (e.g. by increasing the humidity of the gas) the size distribution of the elutriated particles are not affected, but the flux of the elutriated particles increases.

Park and co-workers (2002) increased the relative humidity of the air used to fluidize glass beads from 6 % to 98 %. Park and co-workers (2002) found that the electrostatic charge accumulation decreases if the relative humidity is increased. The preferred relative humidities for decreasing charge accumulation was found to be between 40 % and 80 %. If the air is over-humidified excessive capillary forces were created which resulted in defluidization.

In commercial fluidized bed polymerization reactors charge was found to be successfully eliminated by introducing chemical static agents. The chemical static agents include charge inducing agents such as methanol, water and ethanol

which are positive charge inducing agents and acetone which is a negative charge inducing agent. Some particles in a fluidized bed are positively charged while other are negatively charged. The polarity at the top of the bed is determined by the fine particles and the polarity near the distributor is determined by the larger particles due to particle size segregation. If a positive charge potential is measured a negative charge inducing agent should be added and vice versa (Wang *et al,* 2009). Wang and co-workers (2009) found that the mechanism of water and ethanol to reduce electrostatic potentials was similar.

2.2.3 Effect of particle size on entrainment

From an investigation conducted by Do and co-workers (1972) it was found that large particles reach higher heights in the freeboard than smaller sized particles even though the smaller sized particles spend a greater amount of time in the freeboard than the larger particles. It was also concluded that as the superficial gas velocity was increased, the height reached by the particles as well as the residence time in the freeboard also increased independent of particle size.

Numerous models that were developed to determine the flux of entrained solids made the assumption that the losses due to entrainment are proportionally larger for the fine particles than the larger particles in a bed of multisize particles (Briens *et al*, 1992).

2.2.4 Effect of bed height and column diameter on entrainment

According to an investigation done by Baron *et al* (1990) the height of the bed in the column significantly affect the entrainment flux. With an increase in bed height the entrained flux also increased with as much as 15 % when the bed height was doubled. It was also found that no matter what the superficial gas velocity was the same increase in entrainment was observed for the same increase in bed height. The increase in entrainment flux was attributed to an increase in the amount of particles that were ejected from the bed surface and because there is an increase in bubble size with bed height (Yang, 2003: 119).

According to a study made by Lewis *et al* (1962) (quoted by Yang (2003: 118)) it was found that if the diameter of a fluidization column is larger than 10 cm the entrainment is not influenced if the column diameter is changed. Entrainment is less for fluidization columns with a diameter smaller than 10 cm when compared to a fluidization column with a larger diameter (during the investigation a 7.6 cm column and a 15.2 cm column was used).

2.2.5 Effect of temperature and pressure on entrainment

Choi *et al* (1999) derived a correlation to determine the effect of temperature on the entrainment rate, they neglected interparticle forces. Choi *et al* (1999) concluded that the entrainment rate reaches a minimum value when the gas temperature is increased (valid temperatures: 12 °C to 600 °C). Choi *et al* (1999) explained that this trend results due to the gas density that decreases (therefore also a decrease in the terminal velocity of an individual particle) and the gas viscosity that increases with increasing temperature. According to Choi *et al* (1999) the entrainment rate increases when the gas pressure is increased (valid pressures: 101 kPa to 3200 kPa). The particles used to verify the correlation developed by Choi *et al* (1999) have densities between 2400 kg/m^3 to 6158 kg/m^3.

2.2.6 Effect of particle shape on entrainment

From an investigation conducted by De Vos, Nicol & Du Toit (2009) on different shaped ferrosilicon particles (high-density Geldart group A particles) it was concluded that the entrainment rate is higher for particles that are less spherical, but De Vos *et al* (2009) also found that at very small particle diameters (< 25 µm) the entrainment was higher for the more spherical particles. The conclusion was made that particle shape influences entrainment characteristics.

There are multiple factors influencing the entrainment rate as discussed in Sections 2.2.1 to 2.2.6. The choices made regarding the fluidized bed parameters and particle properties are given and discussed in Section 3. The

entrainment measurement device developed in this investigation was verified by focusing on Section 2.2.2. Based on the findings by Wang and co-workers (2009) regarding the elimination in charge that could be obtained when ethanol is injected into the air feed stream; the entrainment measurement device was used to determine if a change in the electrostatic potential of the fluidized bed and therefore the entrainment could be observed as discussed in Section 5.

2.2.7 Determination of entrainment rates

There are many approaches that can be used to determine the entrainment rate. The entrainment rate can be estimated using an empirical correlation or measured using one of the measurement techniques developed by previous investigators. In this section some of the methods used to estimate the entrainment rate and different measuring techniques used to measure mass flow rate are discussed.

2.2.7.1 Models

A great deal of correlations were developed in order to calculate the flux of entrained solids, but in order to use these correlations the conditions must be the same as the conditions used in the development of these correlations (Briens *et al*, 1992).

The gas exit from a fluidized bed is usually located at a height greater than the TDH, since this economically desirable location is where the solids concentration is at its minimum (Kunii & Levenspiel, 1991: 173). There are two main methods that are used to determine the entrainment rate for columns with a freeboard height greater than the TDH. Both methods make the assumption that the entrainment rate of a particular sized particle is directly proportional to the weight fraction of the same sized particle in the bed.

The first method requires that the size distribution of the bed be divided into intervals in order to determine which particle sizes has terminal velocities less

than the superficial gas velocity; since it is mostly these sized particles that will be entrained. The maximum flux of the particles that can leave the column at a height greater than the TDH (with the assumption that the entire bed consists of particles of the same size) can be calculated using a dimensionless plot given by Kunii & Levenspiel (1991: 175). The maximum flux is then multiplied with the weight fraction. The same procedure is repeated for all elutriable particle sizes and then the sum is taken of the resulting values to give the total entrainment rate (Kunii & Levenspiel, 1991: 174).

The second method is based on the elutriation rate constant which is the same as the maximum flux of a particular sized particle when the bed only contain particles of the same size. The elutriation rate constant is a true rate constant and is not affected by changes in the weight of the bed. The elutriation rate constant is determined experimentally either through a solids flow experiment or batch experiment. The weight fraction of all elutriable solids in the bed and the carry-over rate must be known in the former case and the weight fraction of each elutriable particle initially in the bed and after the fluidized bed was operated for a certain amount of time must be known in the latter case. Correlations developed for the elutriation rate constant by previous investigators can be used to determine the elutriation rate constant. The elutriation rate constant calculated for each size is then multiplied with the weight fraction of the corresponding size. The sum is taken of the resulting values to give the total entrainment rate (Kunii & Levenspiel, 1991: 175-177).

2.2.7.2 Measurement techniques

Apart from the correlations available to determine the entrainment rate other techniques can be used to determine the entrainment rate for external circulating fluidized beds. These fluidized beds are operated with a net solids flux of 10 kg/(m^2.s) to 1000 kg/(m^2.s). Assuming plug flow in the downcomer from the cyclone the entrainment rate can be determined by timing the decent of the particles along the wall of the downcomer. A rough downcomer leads to an

underestimated entrainment rate due to the particles being retarded at the downcomer surface. Three other methods that can be used to determine the entrainment rate is by closing a perforated butterfly valve in the downcomer and determining one of the following:

- the time needed to accumulate a certain volume of solids;
- the time needed to obtain a certain pressure drop across the bed of solids which collects above the valve;
- the rate of decent of the packed bed level below the valve in the downcomer.

A shortcoming of these methods is that the pressure balance of the system is disturbed, since the particles are diverted (Yang, 2003: 498-499).

In an investigation conducted by Liu, Takafuji and Suda (2011) on the effect of riser scale on the hydrodynamics and particle residence time distribution; the entrainment rate was determined by making use of a sensor placed in the cyclone dipleg. The sensor measures the impact of the separated solids as the solids fall on a detection plate. The entrainment fluxes used in the experiments were between 10.1 kg/(m^2.s) and 26.6 kg/(m^2.s).

An impact plate was used by Harris, Davies & Davidson (1997) to measure the flow rate of a stream of particles. The impact plate deflects the particles when they come into contact with the plate. The deflection causes the particles to undergo a change in momentum. The change in momentum can be correlated against the flow rate of the particles. Measurement using an impact plate makes measurement difficult due to the uncertainty that exist whether an impact was elastic or inelastic. The reactive force caused by elastic impacts is twice the reactive force caused by inelastic impacts (Harris *et al*, 1997).

Solids flow rate was also determined by measuring the pressure drop after the solids flowed through a 90 degree elbow at the top of the column of a circulating fluidized bed. The pressure drop was correlated with the flow rate, but extensive

calibration was needed (Harris *et al*, 1997).

Local mass flux can be measured in the riser of a circulating fluidized bed using piezoelectric pressure transducers. The particles strike the active region of the pressure transducer causing spikes in the voltage measurements. Each spike corresponds to one particle strike. The number of spikes is counted giving the total number of particles which would have passed through the area taken up by the detector during a specific time interval. The mass flow rate is calculated from the number of particles counted, particle density, particle size and the area occupied by the detector. A piezoelectric pressure transducer was used in the riser of a fluidized bed containing polyethylene particles, the fluidized bed was operated at solids circulation rates between 19.4 kg/(m^2.s) and 155.5 kg/(m^2.s). Interference with the solids flow was experienced when the probe was used to sample fluxes beyond the centerline of the riser due to the large size of the probe (Spenik & Ludlow, 2010).

The overall mass flux was measured in a circulating fluidized bed by tracking a single radioactive particle. The radioactive particle was made the same size and density of the glass beads used in the investigation (particle density and mean particle diameter were 2550 kg/m^3 and 150 µm respectively) by coating the particle with a layer of polymer. The mass flux was determined from the solids velocity which was estimated using two NaI (TI) scintillation detectors and the solids holdup which was measured using γ-ray line densitometry (Bhusarapu, Al-Dahhan & Dudukovic, 2004a). Using radioactive particle tracking Bhusarapu and co-workers (2004b) were able to establish a calibration curve for an overall solids mass flux in the range of 10 kg/(m^2.s) to 35 kg/(m^2.s).

Mass flow rate measurement in pneumatic transport systems

Research that has been done on the measurement of the mass flow rate of solids in pneumatic transport systems is mainly divided into two sections namely indirect measurement and direct measurement. With indirect measurement the

solids concentration and the solids velocity must be known in order to infer the mass flow rate of the solids. With direct measurement a sensor is generally used which is directly influenced by the mass flow rate of the solids (Zheng & Liu, 2011).

Techniques used for indirect measurement is divided into the techniques required to measure the solids concentration and the techniques required to measure the solids velocity. The following are some of the techniques used to measure solids concentration (Zheng & Liu, 2011):

- *Capacitance sensors:* The capacitance is measured over a sensor as the solids flow through the sensing field of the sensor.
- *Optical sensors*: Based on the measurement of the amount of light that is reflected by the particles in the system the solids concentration can be determined.
- *Acoustic sensors*: In dilute pneumatic transport systems sound waves can be used to measure the solids concentration. The waves are introduced into the pipeline at a certain frequency and the propagation of the waves over a certain axial length is measured. The solids concentration is determined from the relationship between the axial attenuation of the waves and solids concentration.

Many methods were developed to measure the solids velocity. Sensors (optical, capacitance, electrostatic etc.) can be used in combination with correlation analysis or together with spatial filtering techniques (Zheng & Liu, 2011).

In this investigation the focus is on the development of a mass flow meter which is based on direct measurement techniques.

Some of the techniques used for direct measurement are based on the heat transfer principle or Coriolis force. Thermal methods include (Zheng & Liu, 2011): measuring the increase in the temperature of the solids as they move through a

warm region which was obtained by constant heat input to the region or by measuring the amount of heat needed to maintain a fixed temperature difference. In a dense pneumatic transport system the solids flow rate was determined from the relationship between the mass flow rate, the temperature difference between the inlet and outlet of a heated section of pipe and the heat transfer coefficient. The heated section of pipe was obtained by passing a current through a resistance wire which was wounded around the pipe on the outside. The method was applied to a vertical pipeline (diameter is 0.0175 m) for mass flow rates in the region of 0 kg/h to 1000 kg/h. A drawback of the abovementioned method is that heat transfer must occur through the wall of the pipeline and this heat transfer must be characterized (Zheng & Liu, 2011).

In a dilute phase pneumatic transport system the mass flow rate was determined by placing two sensors in the pipeline. One sensor was used for heating and sensing and the other sensor was just use for sensing purposes. A feedback control circuit was used to maintain a constant temperature difference between the process temperature and the sensor used for heating. The amount of electrical power needed to ensure the temperature difference stayed constant was measured and related to the mass flow rate of the solids. The drawbacks of this method are that the sensors were damaged by attrition in the pipeline and mixing of solids and gas must be as uniform as possible, therefore there should be at least 15 m pipeline between the sensing region and the mixing point of the solids and gas (Zheng & Liu, 2011).

Slot flow meter

A solid mass flow meter or slot flow meter was developed by Harris and co-workers (1997). The flow meter consists of a perforated cylindrical metal container which is open at the top and closed at the bottom. The perforations are vertical slots. A cone is placed inside the container to canalise the solids to flow through the slots and thereby preventing stagnant regions. The slot flow meter is mounted on a load cell which measures the inventory of the container. The mass

flow rate of the solids is related to the powder depth upstream of the vertical slots which in turn is related to the weight of the solids in the container.

Coriolis flow meters

Coriolis flow meters are used to measure the mass flow rate of solids. The Coriolis flow meter consists of a rotating disc with radial vanes. The vanes cause the solids to flow in a radial direction. The resulting torque is measured which is related to the mass flow rate of the solids. The disadvantage of using a Coriolis flow meter is that moving parts and drive shaft seals are necessary if the flow meter is used in a dusty environment (Harris *et al*, 1997).

Thermal mass flow meter developed by De Vos and co-workers (2010)

From the literature discussed in this section it seems that most of the techniques for measuring the mass flow rate are applicable to high solid fluxes of between 10 kg/(m^2.s) to 1000 kg/(m^2.s) (Yang, 2003:498-499; Liu *et al*, 2011; Spenik & Ludlow, 2010; Bhusarapu *et al,* 2004a; Bhusarapu *et al,* 2004b). A thermal mass flow meter, specifically for use in bubbling fluidized beds with relatively low entrainment fluxes, was developed by De Vos and co-workers (2010). The entrainment fluxes investigated were approximately between 1 x 10^{-3} kg/(m^2.s) and 16 x 10^{-3} kg/(m^2.s).

This measurement device used the principles of a thermal mass flow meter. The measurement device consisted of a rectangular copper plate which was heated and placed in the dipleg below the cyclone. Heat transfer takes place mainly through conductive heat transfer between the particles and the heated metal plate. The plate was heated and the temperature of the plate measured by thermally connecting two electronic circuits to the plate. One circuit was a thin wire heated by sending an electric current through the wire and the other circuit used a thermistor, the resistance of this electronic component changes with temperature, which causes changes in the voltage measurements made across this circuit (De Vos *et al*, 2010).

The measuring device was calibrated for glass beads with a density of 2600 kg/m^3 and a mean particle size of 138 µm by collecting the solids below the measuring device. The mass of the collected solids was determined and the integrated voltage reading obtained during the time the solids were collected was taken. De Vos *et al* (2010) made a calibration plot of the recorded voltage over the measuring device and the flux of solids. A disadvantage of the measuring device is the nonlinearity of the calibration curve at higher entrainment rates which implies a loss in sensitivity of the measurement device. The loss in sensitivity to changes in the inferred temperature is due to a decrease in the temperature gradient available for heat transfer as the amount of cooling of the measurement device increases (Nicol, 2011).

3. Experimental

In order to determine the entrainment rate, a fluidized bed with external recycle and a solid mass flow meter were used. In Sections 3.1 and 3.3 the fluidized bed and the solid mass flow meter are discussed respectively.

3.1 Fluidized bed

3.1.1 Apparatus

A fluidized bed similar to the fluidized bed used by De Vos *et al* (2010) was designed. A schematic diagram of the fluidized bed setup is shown in Figure 2.

The fluidized bed consists of a 190 mm inner diameter Perspex column with a wall thickness of 5 mm. The height of the column is 6093 mm. The column is divided into four sections for cleaning and maintenance purposes. The fresh particle feed pipe connects to the second section from below and is tightly sealed during operation. Properly earthed copper wires are coiled around the column, plenum chamber and connecting bolts. The column has multiple ½'' and ¼" NPT (national pipe thread) pressure tappings.

The grid plate is a typical plate grid made of mild steel with a thickness of 5 mm and with 69 holes (diameter 2 mm) arranged in a triangular pitch. The pressure drop across the plate is higher than 30 % of the pressure drop across the bed for all linear velocities. Synthetic filter material from HISAClean (type VPB 751) was placed beneath the metal grid in order to prevent the weepage of solids through the grid plate into the plenum chamber.

Air was supplied by the utility services of the nuclear energy corporation of South Africa (Necsa). The air was available at a pressure of 650 kPa(g) to 750 kPa(g). Air was taken from two points from the main air supply line. The dipleg and cyclones are supplied with air from one supply point and the fluidization column

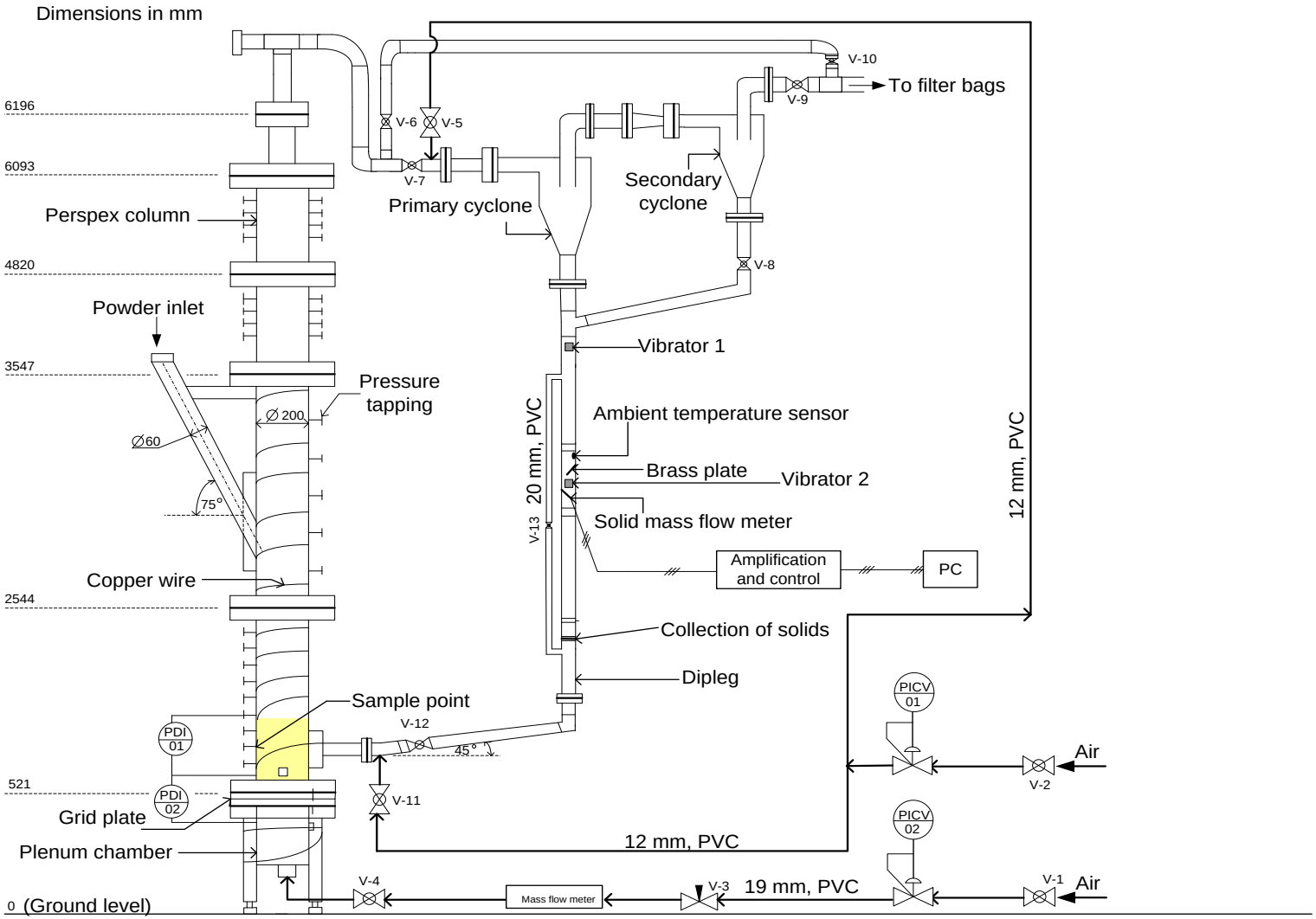

Figure 2: Schematic diagram of fluidized bed setup.

is supplied with air from the other supply point. The air to the fluidization column was regulated using a standard ½'' pressure regulator (PICV 02) from Wika instruments and the air to the cyclones and the dipleg was regulated using a standard ½" pressure regulator (PICV 01) from Rhino valves. Both pressure regulators were set at1 bar (g) and kept at that pressure except when more air was needed at higher linear velocities. A needle valve (valve V-3) was used to adjust the flow rate of air to the column. All other valves are ordinary ball valves.

Flexible PVC pipelines were used for the air lines and the sizes were chosen so that the linear velocity in the lines does not exceed 100 m/s and is not below 5 m/s to prevent problems of possible corrosion and the development of static charges (Greeff & Skinner, 2000: 79). The rest of the pipelines are made of poly(vinyl chloride) (PVC) and have an inner diameter of 45 mm (50 mm outer diameter), except for the inlet to the secondary gas cyclone which has an inner diameter of 35 mm (40 mm outer diameter).

Air was introduced into the dipleg by opening valve V-11 in order to fluidize the powder in the dipleg and to facilitate the recycle from the cyclone back to the bed. Additional air is fed into the inlet line of the primary gas cyclone in order to increase the inlet linear velocity to each gas cyclone to at least 15 m/s (especially at low air flow rates to the column); which is seen as the optimum inlet velocity for high efficiency cyclones (Sinnot, 2005: 453). Two cyclones made of Perspex (cone section made of PVC) were used in series in order to increase the solids removal efficiency (Rhodes, 1998: 175-187). Carry-over solids from the secondary cyclone were removed from the air stream by three filter bags placed downstream of the secondary cyclone. The filter bags are ordinary vacuum cleaner bags, type VPB 751 from HISAClean.

The pressure drop across the bed and the pressure drop across the grid plate were measured using two Wika DP-10 differential pressure transmitters (PDI 01 and PDI 02 respectively). These transmitters have a measurement range of 0 bar

to 1 bar and an accuracy of 0.01 bar. The volumetric flow rate of the air entering the column was measured using an in-flow mass flow meter, type F-116Al-AGD-55-V, from Bronkhorst. The accuracy of the mass flow meter is ± 0.8 % of the reading plus ± 0.2 % of full scale (measurement range 0 l/s to 30 l/s) (In-Flow, *sa*). A LM35 temperature sensor was placed in the dipleg beneath the gas cyclones in order to determine the temperature of the environment around the solid mass flow meter. At room temperature the accuracy of the temperature sensor is ± 0.25 °C, and in the temperature range -55 °C to 150 °C the accuracy is ± 0.75 °C (National Semiconductor, 2000). The relative humidity of the air was measured using a SHT75 relative humidity sensor with an accuracy of ± 1.8 % (Sensirion, 2010). The humidity sensor was placed inside the column near the wall in the third section from below.

Two vibrators were attached to the column (see vibrator 1 and vibrator 2, Figure 2). These vibrators were used to minimize powder buildup on the walls of the dipleg and on the brass plate in the dipleg. The brass plate in the dipleg was used to canalise the powder onto the metal plate of the solid mass flow meter. The solid mass flow meter is described in detail in Section 3.3. Below the solid mass flow meter a circular PVC disc was placed in the dipleg in order to collect the solids from the cyclones for calibration purposes. The collected solids are removed from the dipleg by removing the connections that connect the 200 mm section of pipe which contains the shut off disc to the dipleg. A 20 mm PVC gas bypass line was used around the shut-off disc in order to prevent pressure buildup in the system. Collected solids from calibration experiments were weighed with a scale from the Denver Instrument Company; model TR 2102 which can measure the mass of the solids to a mass difference of 0.01 g.

Samples were taken from the bed at the sample point shown in Figure 2 in order to determine the particle size distribution of the bed. The particle size distribution was measured using Mastersizer 2000 version 5.21 from Malvern instruments.

3.1.2 Physical and chemical properties of fluidization material and fluid

Starbead® industrial beads were used as the bed material. The physical and chemical properties of the industrial beads are given in Table 2 (MSDS, 2003). The particle size distribution of the bed particles is given in Figure 3. The Sauter mean diameter of the particles is 133 µm. The fluid used to fluidize the glass beads is air at ambient conditions, approximately 25 °C and 1 bar. The humidity of the air received from Necsa varied depending on the season. Before the rainy season the humidity was between 11 % and 12 % and during the rainy season the humidity was between 38 % and 40 %, but remained approximately constant from day to day within a season. The results given in Section 4 were obtained before the rainy season.

Table 2: Physical and chemical properties of fluidization material

Property	Description/value	Unit
Material	Soda-lime-silica glass	
Melting point	± 730	°C
Specific weight[A]	± 2.6	g/cm^3
Bulk weight[A]	± 1.6	kg/L
Appearance	Transparent round particles	

[A] Taken from Blastrite (2011)

3.1.3 Operation of fluidized bed

The fluidized bed was filled with powder up to a bed height of 80 cm in order to ensure that the entrainment measurements were made at a height above the TDH. Using Equation 7 the TDH was calculated as 78 % of the freeboard height at a superficial air velocity of 0.7 m/s. The fluidized bed was operated at superficial air velocities from 0.2 m/s to 0.7 m/s. After fluidizing the bed, the bed height was measured as 76.5 cm. The powder in the dipleg was 4.4 % (mass) of the fresh particle feed. The same batch of powder was used to generate the

results given in Sections 4 and 5.

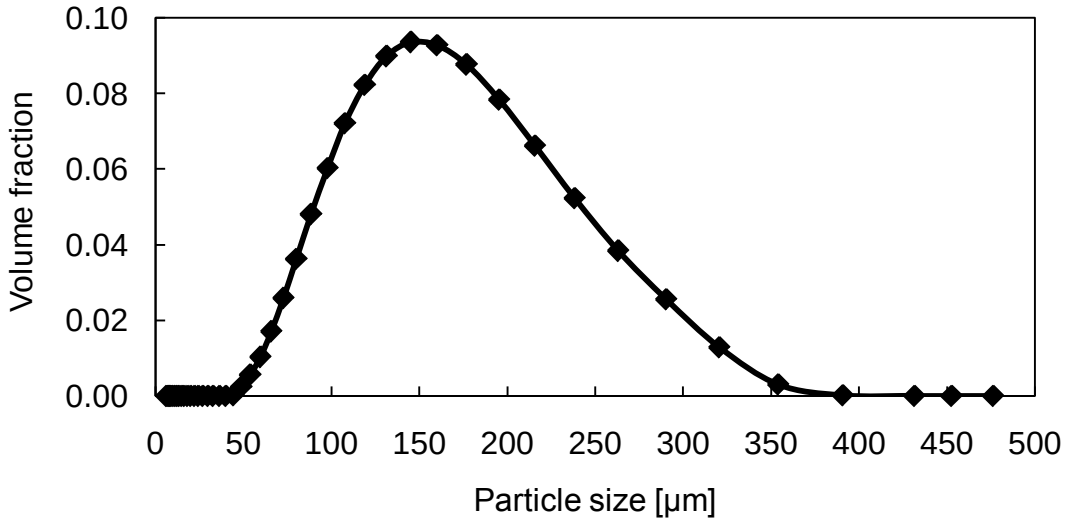

Figure 3: Particle size distribution of the bed particles.

The Geldart chart indicates type B particles and accordingly the minimum fluidization velocity was determined by detecting initial bubble formation. A value of 8 mm/s was determined. At minimum fluidization the distributor pressure drop was 37 % of the bed pressure drop (8.4 kPa). This fraction increased to 72 % at the maximum investigated superficial velocity (0.7 m/s).

Using Equations 5 and 6 the velocities u_c and u_k were calculated; u_c has a value of 1.37 m/s and u_k is equal to 2.13 m/s. As discussed in Section 2.1.2 u_k is usually used as the velocity corresponding to the transition velocity between the bubbling regime and turbulent regime of fluidization. The fluidized bed was operated at a maximum air velocity of 0.7 m/s which is well below u_c and u_k; to ensure that all the experiments were done in the bubbling fluidized regime.

Fluidization startup

Before the glass beads in the bed of the fluidization column can be fluidized, the following procedure was followed: Valves V-1 to V-3, V-6, V-10 and V-11 were kept closed and valves V-4, V-5, V-7, V-8, V-9 and V-13 were opened fully

(Figure 2). Ball valve V-12 was always kept open. Thereafter air was introduced into the inlet line of the primary gas cyclone by fully opening ball valve V-2. Ball valve V-11 was opened slightly until the powder in the dipleg was completely fluidized and then the valve was kept open in that position.

Fluidization of glass beads

In order to start the fluidization of the glass beads, needle valve V-3 was opened until the mass flow meter reading corresponds to the desired linear velocity. Both vibrators were then switched on. The pressure readings from the differential pressure transmitters (PDI 02 and PDI 01, Figure 3) were monitored in order to ensure that there is good gas distribution across the grid plate and to determine the pressure drop at minimum fluidization.

Fluidization shutdown

After the glass beads were fluidized for the required time duration, needle valve V-3 was closed first, followed by ball valve V-11 and then ball valves V-1 and V-2. The rest of the valves were then closed. The three filter bags, where the unseparated solids are collected, were then examined to ensure that they were not full in which case they were replaced. After replacement of the filter bags the unseparated solids were returned to the column. After each calibration experiment the collected solids were returned to the bed.

3.2 Solid mass flow meter

3.2.1 Design

The design of the solid mass flow meter was based on a selective combination of the flow meter developed by De Vos *et al* (2010) (refer to Section 2.2.7.2) and constant temperature anemometry as explained by Lötters (1999).

Constant temperature anemometry requires the use of a heater resistor as well as a temperature sensing resistor. These resistors must be made of temperature

sensitive resistive material. The resistors are each placed inside a stainless steel tube. The tubes are then placed inside the flow of gas; each through a small hole in the pipeline through which the gas flows. The two resistors are connected in a Wheatstone bridge configuration. An electric current is sent through the heater resistor and a current is sent through the temperature sensing resistor, this causes the temperature of the heater resistor to rise e.g. 30 °C above ambient temperature, while the temperature sensing resistor is used to measure ambient temperature (Lötters, 1999).

The Wheatstone bridge configuration provides the heater with the heater current and the sensor with the measuring current, but when the equilibrium of the bridge is disturbed (the difference in temperature between the heater and the sensor is not equal to e.g. 30 °C due to heat transfer to the gas) an error voltage is produced. A proportional-integral (PI) controller then adjusts the heater current in order to ensure the equilibrium is restored. The heating power necessary to restore equilibrium is a function of the mass flow rate of the gas. A schematic diagram of the Wheatstone bridge configuration is given in Figure 4 (Lötters, 1999).

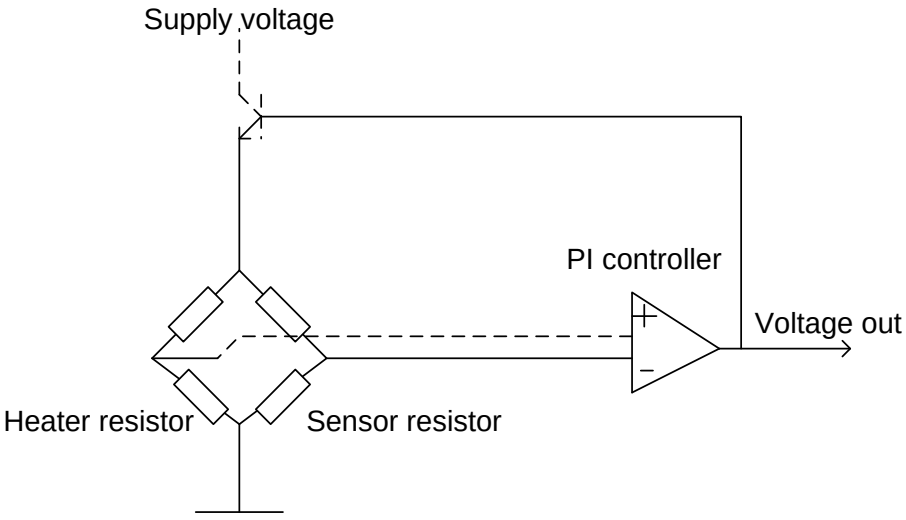

Figure 4: Wheatstone bridge (taken from Lötters, (1999)).

The solid mass flow meter developed in this investigation was different in the following aspects:

- Instead of using a change in the resistance to infer a change in temperature as was reflected in the voltage measurements made by De Vos *et al* (2010), the temperature of the measurement plate was measured directly using temperature sensors. A constant temperature difference (between the plate and the environment) was used rather than using a constant heat input to the plate.
- Instead of using resistors in a Wheatstone bridge configuration as was done by Lötters (1999) the resistors were connected in series. The plate temperature was the controlled variable compared to the equilibrium of the Wheatstone bridge which was used by Lötters (1999) as an indication of a temperature change of the heater resistor.

The solid mass flow meter consists of an oval brass plate of thickness 0.05 mm which was placed at an approximate angle of 45 degrees in the dipleg as shown in Figure 5. The plate is attached to the entire inside circumference of the pipe with a small opening on one side. The opening size was determined through trial and error and was chosen to be as small as possible so that the largest possible area of the plate is exposed to the powder without causing clogging and excessive solids buildup. At the cyclone exit the solids flow is canalised onto the solid mass flow meter to ensure proper contacting.

Two LM35 temperature sensors are attached to the bottom of the brass plate (see Figure 5). The sensors were placed at different positions on the plate to monitor the temperature homogeneity of the plate. At room temperature the accuracy of the temperature sensors is ± 0.25 °C, and in the temperature range -55 °C to 150 °C the accuracy is ± 0.75 °C (National Semiconductor, 2000). Also attached to the bottom of the plate are eight 6.8 ohm resistors in series (as indicated in Figure 5).

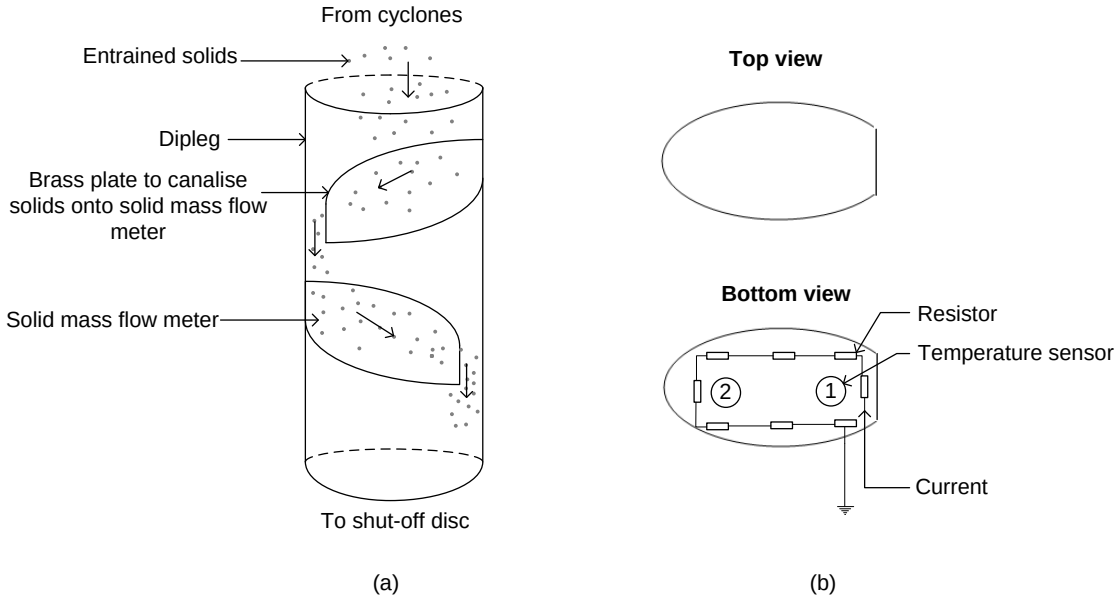

Figure 5: (a) Position and orientation of mass flow meter in dipleg of fluidized bed and (b) top view and bottom view of mass flow meter.

A schematic diagram of the solid mass flow meter is given in Figure 6. The signals from the temperature sensors on the plate and the temperature signal from the ambient temperature sensor (shown in Figure 2) are volt signals, the outputs are 10 mV for each °C measured. The output signals from the temperature sensors are sent to a printed circuit board containing three AD627A amplifiers (see Figure 6). The amplifiers amplify the output signals with a factor of 10. The amplified temperature signals are sent to an Arduino microcontroller (model MEGA 2560) which is used as a temperature controller. Amplification of the signals is needed, since the Arduino temperature controller software works with a higher resolution with input signals that cover the range 0 Volt to 5 Volt (Cilliers, 2011). The software on the temperature controller converts the analog signals from the printed circuit board to digital signals and via an universal serial bus (USB) connection to a personal computer records the two plate temperatures as well as the ambient temperature.

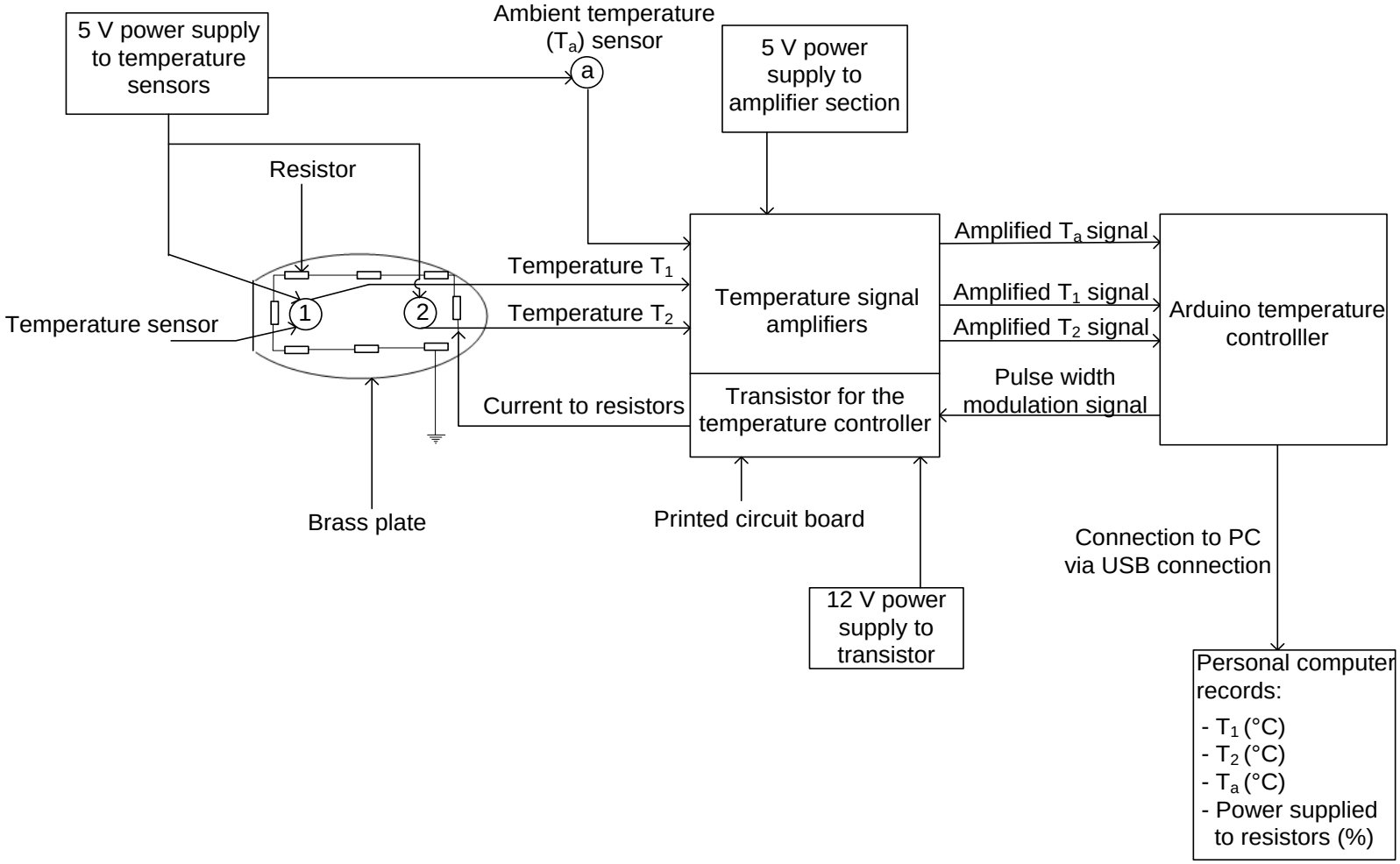

Figure 6: Schematic diagram of the solid mass flow meter.

The temperature of the plate is controlled by modulating the power to the resistors using pulse width modulation (PWM). The software on the Arduino temperature controller calculates the average temperature of the plate using the amplified temperature signals (T_1 and T_2). The Arduino software program requires that a setpoint temperature for the plate and a recording interval be specified.

The software program determines the difference between the measured average temperature of the plate and the setpoint temperature. In order to heat the plate to a certain temperature, the controller sends a square wave signal to the gate of a field effect transistor (FET) located on the printed circuit board. The FET acts as a switch. When the value of the square wave is at a maximum the FET conducts current and when the value of the square wave is at a minimum the FET is not conducting current. The result is that current is sent to the resistors for a time duration which is proportional to the width of the square wave signal from the controller. Depending on the difference between the temperature of the plate and the setpoint temperature, the controller adjusts the width of the square wave signal sent to the FET. A maximum of 2.6 Watt is available to heat the resistors. The Arduino software records the percentage of the maximum power that is used (Cilliers, 2011).

3.2.2 Operation and operating parameters

A constant temperature difference of 7 °C was maintained between the temperature of the environment around the solid mass flow meter (T_a) and the temperature of the brass plate of the solid mass flow meter. A temperature difference is used instead of a fixed setpoint temperature in order to compensate for the change in the environment temperature. The smallest recording interval allowed by the controller was chosen. The recording interval was 4 seconds.

The brass plate was heated to the setpoint temperature. Sufficient time was allowed for the temperature of the brass plate to reach the setpoint temperature.

Normal procedure was then followed for the startup of the fluidized bed as described in Section 3.1.3. The temperature of the brass plate decreases after fluidization startup due to the convective cooling of the upward flowing air. Sufficient time was then allowed for the temperature of the brass plate to return to the setpoint temperature. Thereafter fluidization of the glass beads was commenced using the procedure described in Section 3.1.3. After the glass beads were fluidized for the required time duration, the fluidization shutdown procedure (as described in Section 3.1.3) was followed. The power required to heat the brass plate was recorded as well as the power required to maintain the setpoint temperature during operation. The solid mass flow meter was calibrated using the required power to maintain the setpoint temperature during fluidization and the mass of solids collected.

4. Mass flow meter results

4.1 Data handling

Typical response curves obtained by the solid mass flow meter are given in Figure 7. Major deviation from the average reading for some of the data points is observed. These points are attributed to false temperature readings that cause drastic control action. The incorrect temperature readings were initially thought to be caused by static electricity effects, since the wires, printed circuit board and Arduino temperature controller are in close proximity to the column and dipleg where static electricity is present. The major earthing attempt (as discussed in Section 3.1.1) did however not reduce the scatter nor did it change the entrainment rate (an indication that earthing the equipment was unsuccessful in reducing the static electricity).

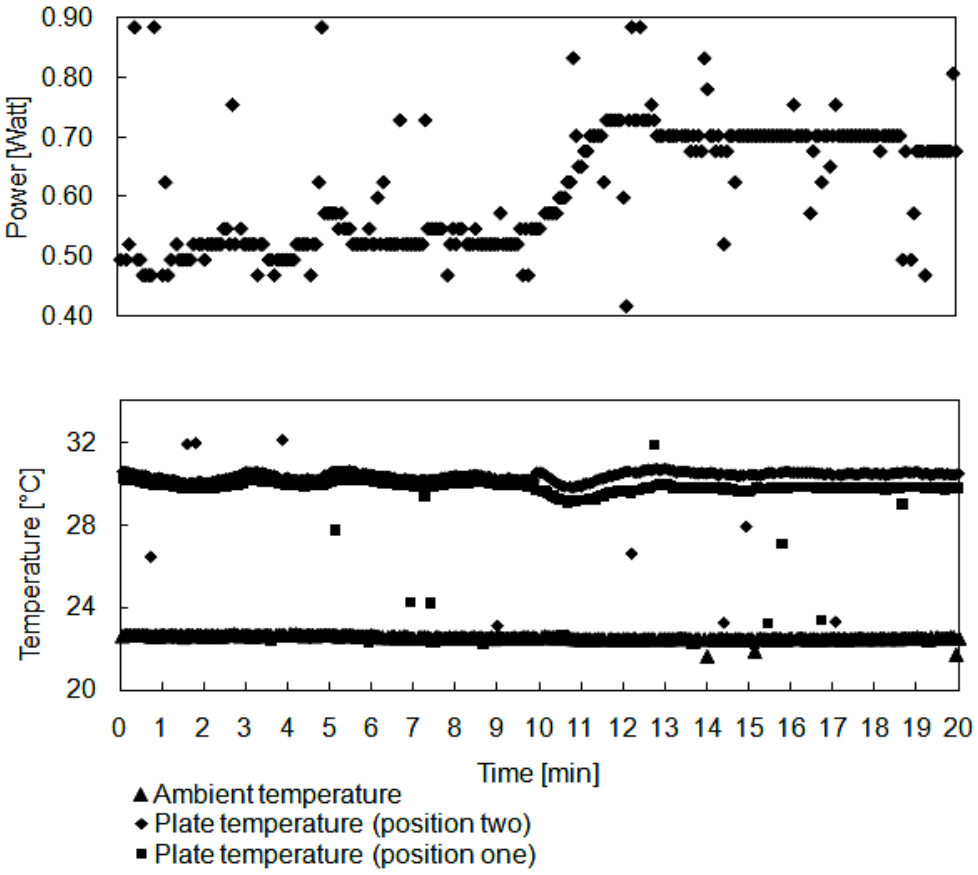

Figure 7: Response curves before filtering.

Although the period of the false temperature reading is unknown, it is likely to be shorter than the sampling rate of 0.25 Hz. It is therefore not possible to follow the complete power (control) response. The total fraction of scatter for the power response is up to five times the total fraction of scatter for the temperature response due to the lagged response of the controller. Since the total fraction of scatter in the temperature readings is small (4.3 % of the temperature data deviated with more than 5 % from the transient mean), it is postulated that the duration of the false readings is short. Accordingly the major scatter points (more than 5 % deviation from the transient mean) were merely removed by a filter. The moving average was taken from the remaining data. Figure 8 gives the response curves generated from the data given in Figure 7 after filtering. The amount of scatter for the rest of the results given in Section 4 was similar to that obtained for the response curves given in Figure 7.

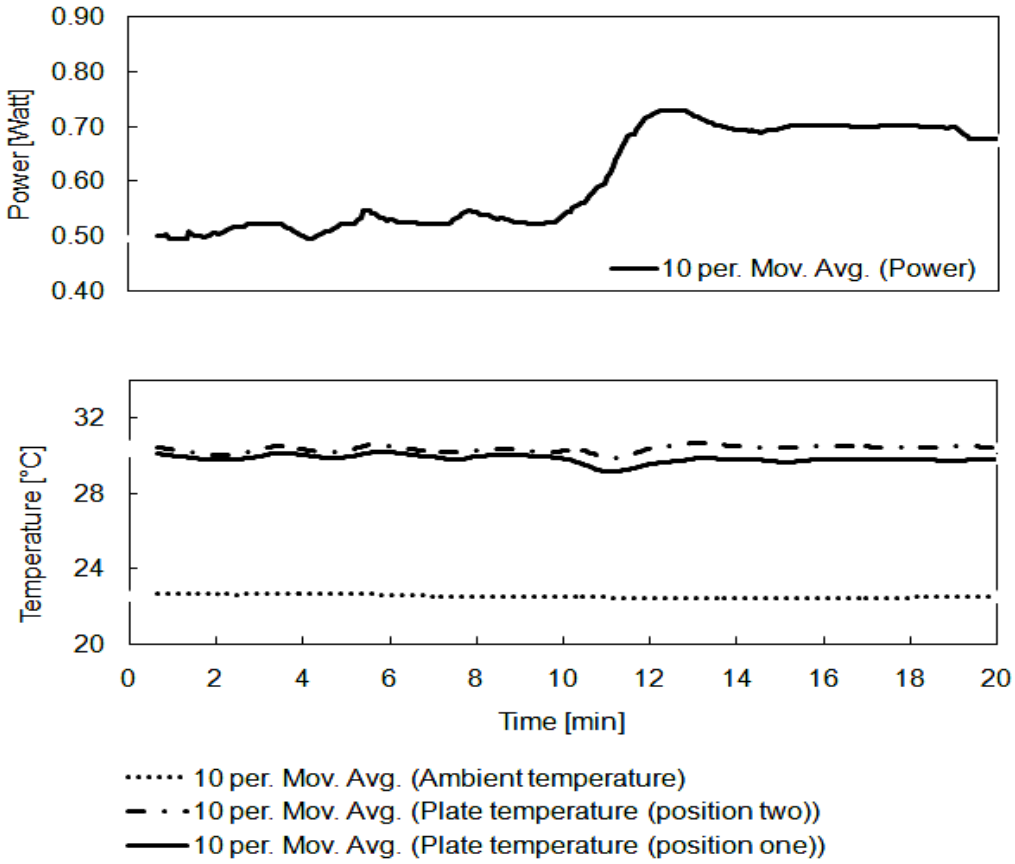

Figure 8: Response curves after filtering.

4.2 Basic response curves

The power response curve obtained after each experiment consists of three regions:

- *Setpoint adjustment without air and solids flow (A):* This section corresponds to the amount of power that is needed to heat the plate and keep the plate at the setpoint temperature.
- *Setpoint adjustment with air flow (B):* The power given in this section is the power needed to keep the plate at the setpoint temperature in the presence of the air from the dipleg.
- *Setpoint adjustment with air and solids flow (C):* The total power needed to maintain the setpoint temperature in the presence of the flowing air (given by region B) and the flow of the separated solids is given in this section.

4.2.1 Low superficial air velocity

The three operating regions are indicated on the response curve given in Figure 9 for a superficial air velocity of 0.2 m/s. In region A it can be seen that approximately 0.52 Watt is needed to keep the plate at the setpoint temperature. A very slight increase in power is observed from region A to B due to the convective heat transfer between the upward flowing air in the dipleg and the mass flow meter plate. Subsequently, the effect of the upward flowing air on the power required to keep the plate at setpoint temperature is assumed to be negligible. Fluidization was commenced and the cooling effect of the entrained solids can be seen in region C (Figure 9). The power increase between region B and C in Figure 9 represents the heat removed by the solids.

Figure 9 shows the two temperatures measured at two different positions on the solid mass flow meter plate. The average temperature difference is 0.62 °C; indicating a near uniform temperature distribution across the plate.

4.2.2 Intermediate superficial air velocity

At an intermediate air velocity of 0.4 m/s the response curve given in Figure 10

was obtained. Similar to the result with the low superficial air velocity, the effect of the upward flowing air was found to be negligible as can be seen from region B in Figure 10. After fluidization was commenced a greater decline in temperature of the mass flow meter plate and a larger increase in power from region B to region C were observed compared to an air velocity of 0.2 m/s.

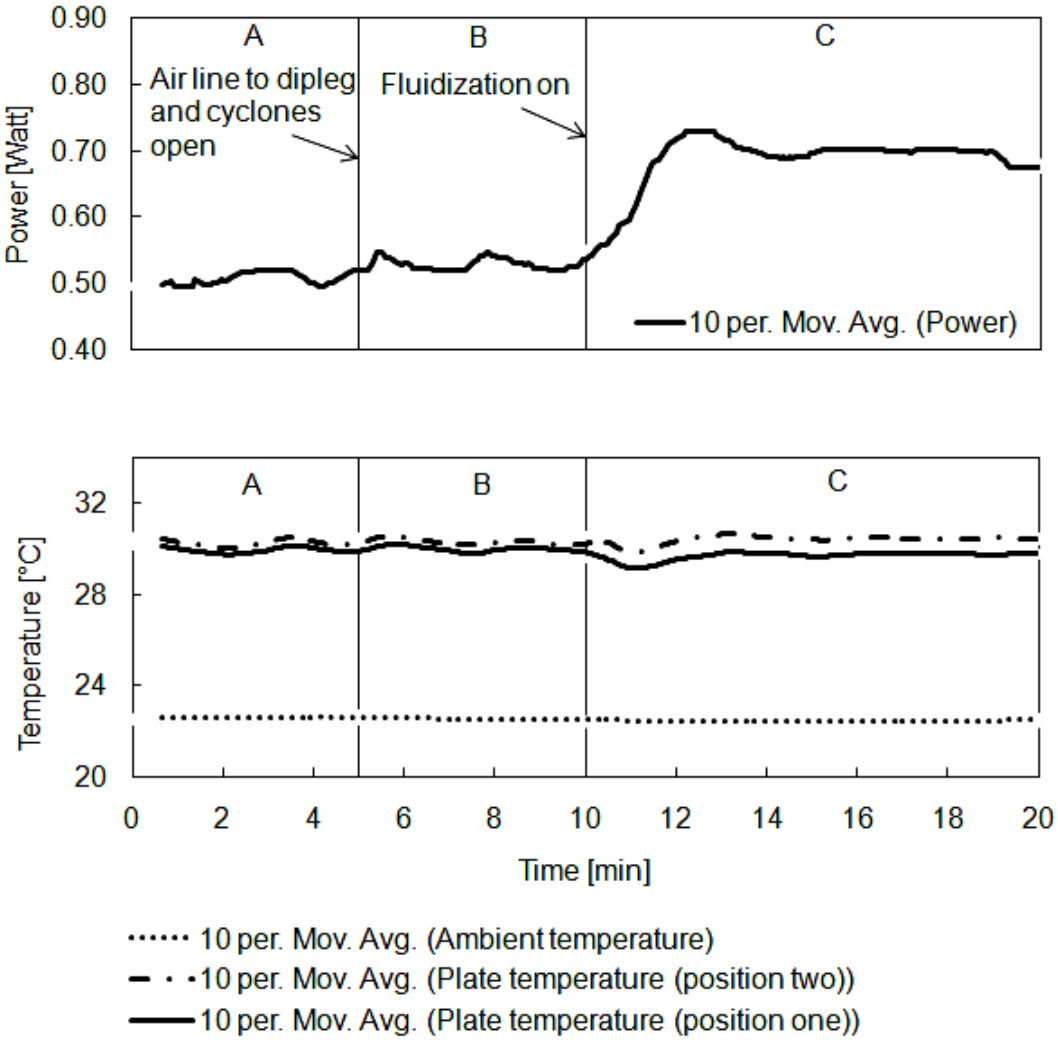

Figure 9: Power usage and variation of temperature over time of the solid mass flow meter at a superficial air velocity of 0.2 m/s.

4.2.3 High superficial air velocity

At a high air velocity of 0.65 m/s the response curve given in Figure 11 was

obtained. After the commencement of fluidization an even sharper incline in the power, as well as a lower dip in the temperature of the mass flow meter plate, than with the intermediate air velocity was observed.

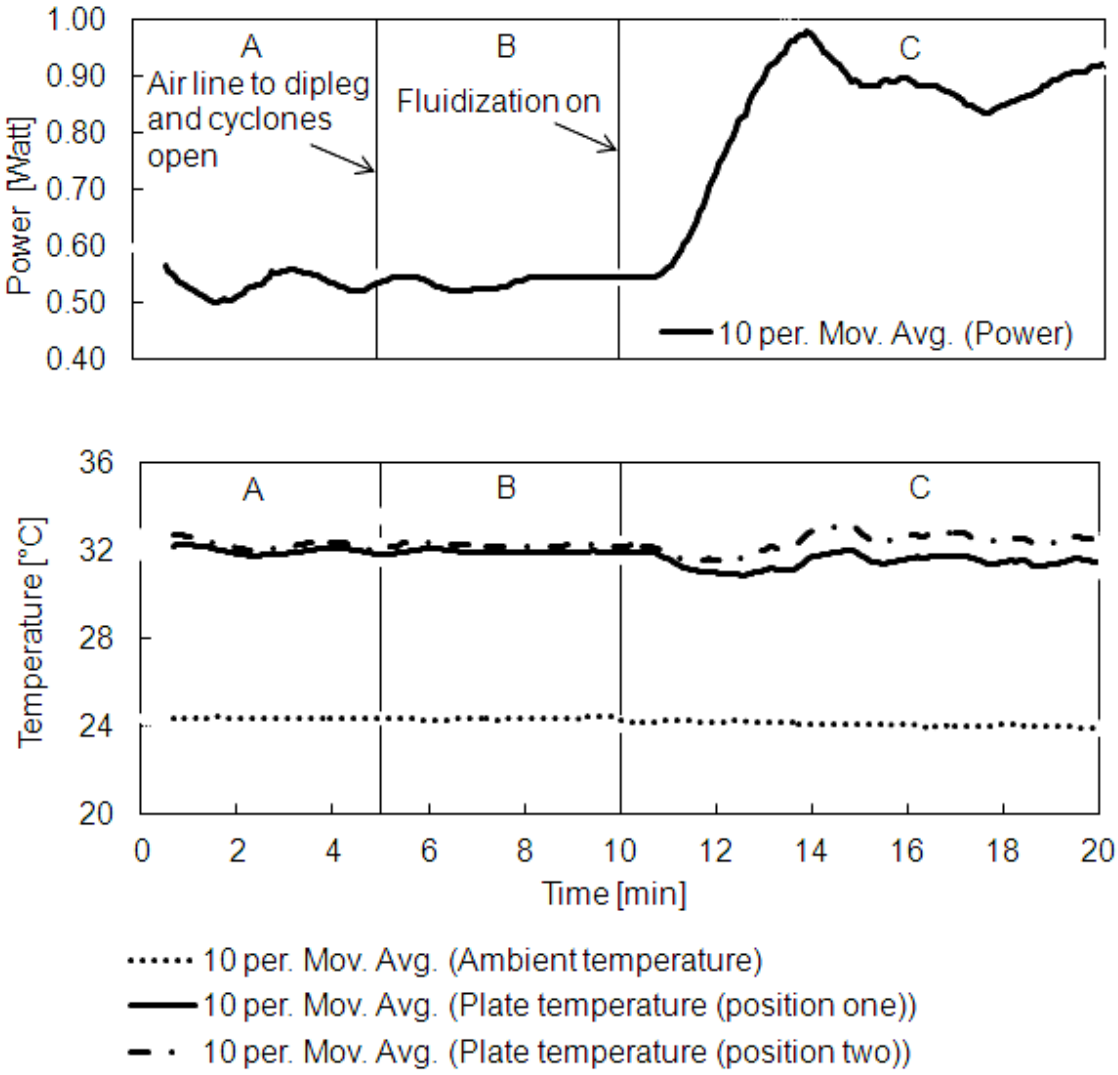

Figure 10: Power usage and variation of temperature over time of the solid mass flow meter at a superficial air velocity of 0.4 m/s.

In region C an overshoot occurs, which was also observed in Figures 9 and 10. The overshoot effect becomes more severe as the entrainment increases. The higher the entrainment, the greater the drop in temperature of the plate which can also be seen in region C of Figures 9 to 11.

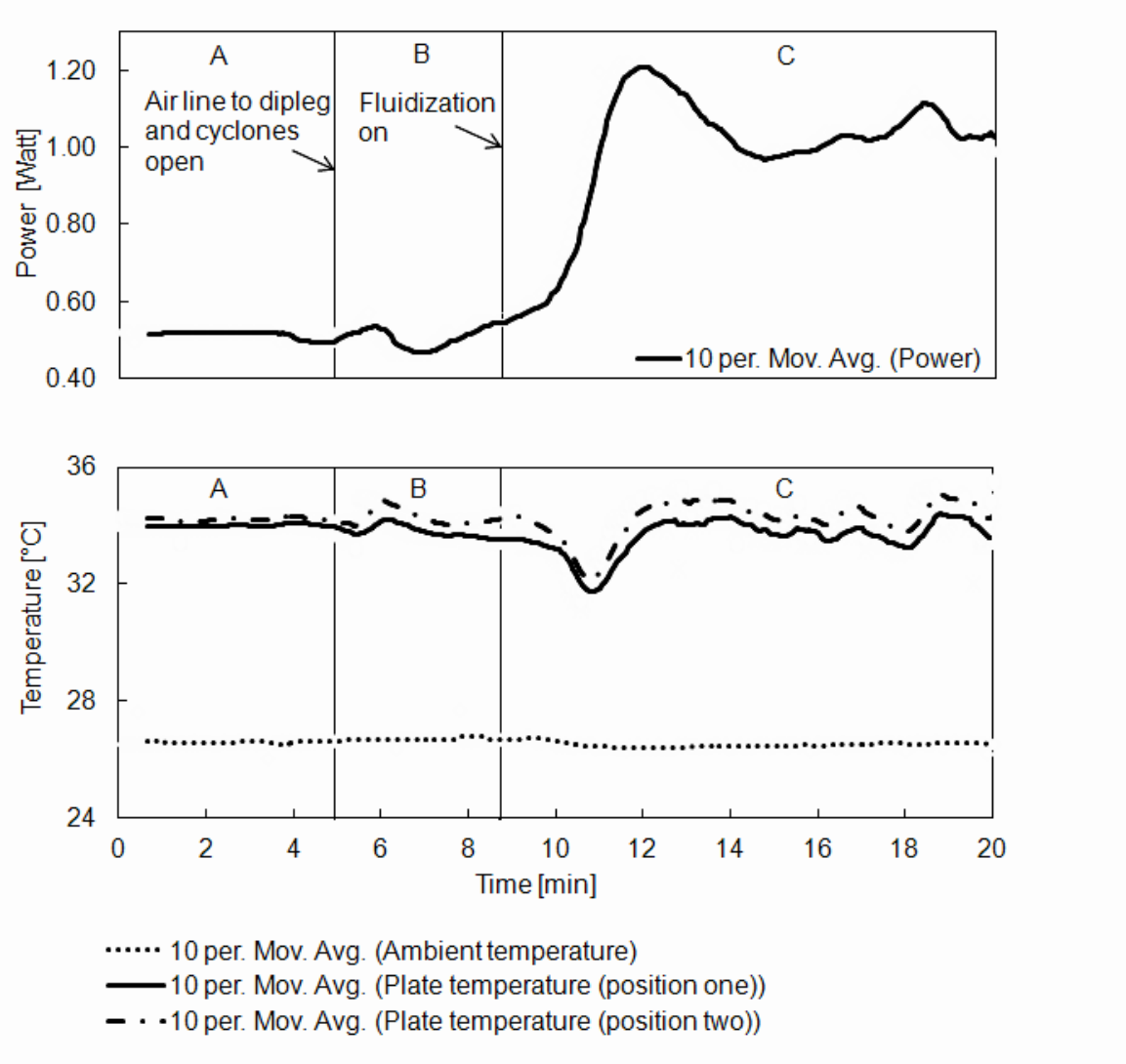

Figure 11: Power usage and variation of temperature over time of the solid mass flow meter at a superficial air velocity of 0.65 m/s.

The inherent dynamics of the heating plate and the relatively slow response of the controller to the sudden cooling effect of the entrained solids (the control system cannot adjust the current as fast as the temperature changes), is the reason for the overshoot in the response curves. When the difference between the plate temperature and the setpoint temperature is smaller the control system performs fast enough to ensure more stable response curves. Due to the significant variation of the plate temperature it is expected that the flow meter will not be accurate at high solids entrainment rates.

4.3 Non solids flow contribution

The total power requirement is divided into two parts, the pre-fluidization power requirements and the during-fluidization power requirements. The pre-fluidization power requirements include the power measured in regions A and B in Section 4.2. The during-fluidization power requirements are discussed in this section.

During fluidization there are three variables that cause the mass flow meter plate to require more power. These variables are:

- the solids flow over the plate;
- additional air entering the dipleg from the column and
- the turbulence in the dipleg caused by the air vortex effect from the exits of the cyclones.

The effect of the additional air and the turbulence on the power requirement can only be estimated from flow experiments with no solids in the column. Therefore only a relative indication can be obtained since the effect may be different in the presence of solids.

Above the distributor a certain fraction of the air entering the column enters the dipleg. The amount of air entering the dipleg increases as the air superficial velocity increases. Figure 12 gives the total power requirement obtained when an empty bed was fluidized at different air superficial velocities for an open and closed dipleg. The dipleg was closed by closing valve V-13 in Figure 2. The difference in the power requirement for an open and closed dipleg was negligible; therefore the additional air entering the dipleg made an insignificant contribution to the total power requirement.

From Figure 12 it can be seen that there is a linear increase in the power requirement with superficial air velocity. The extra power needed due to the turbulence reaches an approximate maximum of 0.18 Watt at 0.7 m/s and a

minimum of 0.05 Watt at 0.2 m/s (Figure 12). At 0.2 m/s the power measurement from the empty column experiment is only 39 % (30 % at 0.7 m/s) of the increase in power from region B to region C of the response curve obtained at the same superficial air velocity. Therefore the turbulence accounts for a 30 % to 39 % contribution to the increase in the power from region B to region C of the power response curve over the experimental velocity range.

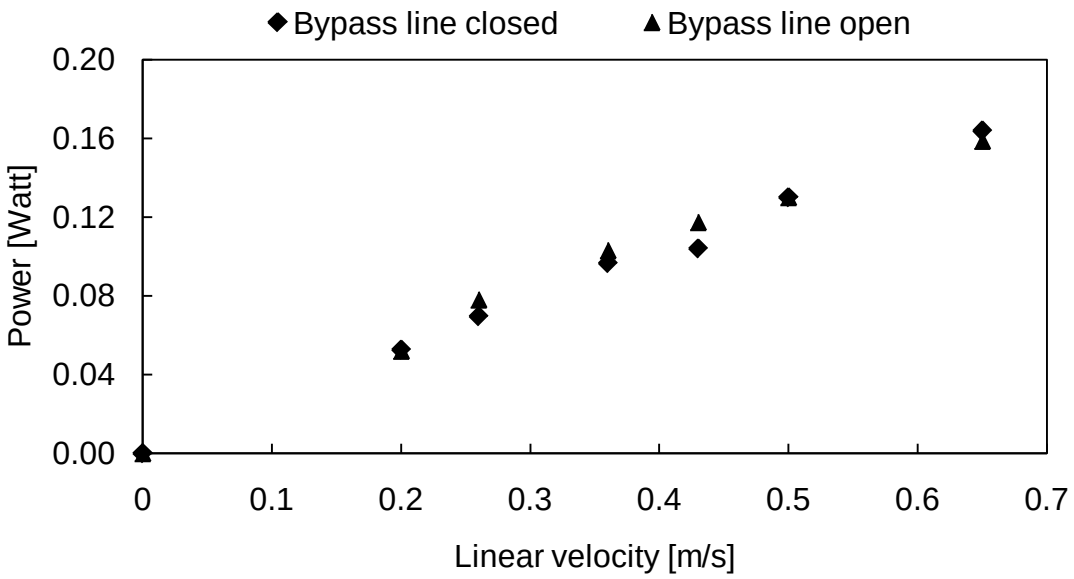

Figure 12: Difference in the power requirement for an open and closed dipleg.

4.4 Calibration

The mass flow meter reading gives the total power that is needed to maintain the setpoint temperature. The total power measurement includes:

a) the power needed to heat the plate to the setpoint temperature and maintain the setpoint temperature (given by region A of the response curve, Section 4.2);
b) the additional power needed to maintain the setpoint temperature due to convective heat transfer caused by the air flow from the dipleg over the mass flow meter plate and which was assumed to be negligible (given by the power increase between region A and B of the response curve, Section 4.2);

c) the heat loss or heat gain from the environment due to a change in the ambient temperature;
d) the power due to the additional air entering the dipleg from the column which was concluded to be insignificant as discussed in Section 4.3;
e) the power due to the turbulence in the dipleg caused by the air vortex effect from the exits of the cyclones; and
f) the additional power needed to maintain the setpoint temperature due to conductive heat transfer between the entrained solids and the mass flow meter plate.

4.4.1 Environmental effects

When the entrainment measurements are done over an extended period of time, the ambient temperature may change significantly from the start to the end of the experiment. In order to compensate for this change in temperature, the difference between the ambient temperature during fluidization and the average ambient temperature before fluidization was calculated. The difference was multiplied by 0.052 Watt / Δ °C as was calculated from the power necessary to increase the temperature of the plate with 1 ºC. The resulting power difference was either added to or subtracted from the measured power values in order to account for the fact that less or more power was required to keep the plate at the setpoint temperature at either warmer or colder conditions respectively.

4.4.2 Corrections made to the response curve

The power required to maintain the setpoint temperature due to the entrained solids (f) was obtained by subtracting the contributions of (a) from the total power measurement and correcting for ambient temperature effects (c) as described in Section 4.4.1. The turbulence caused by the vortex effect (e) was not subtracted from the power measurement; since only a relative indication of the effect is known. However, the relative contribution of this effect, as determined in the absence of solids (see Section 4.3), indicates that the solid flow dominates the

heat transfer from the measurement plate and subsequently also the power requirement.

4.4.3 Calibration curve

The calibration curve was constructed using the power required to maintain the setpoint temperature due to the entrained solids (f). The entrainment flux was calculated from the mass of the solids collected after the column was fluidized for approximately 10 minutes and the area of the column. The calibration data is given in Figure 13. A good linear fit was obtained for the calibration data for intermediate entrainment fluxes between 3.4 x 10^{-4} kg/(m^2.s) and 7.5 x 10^{-3} kg/(m^2.s).

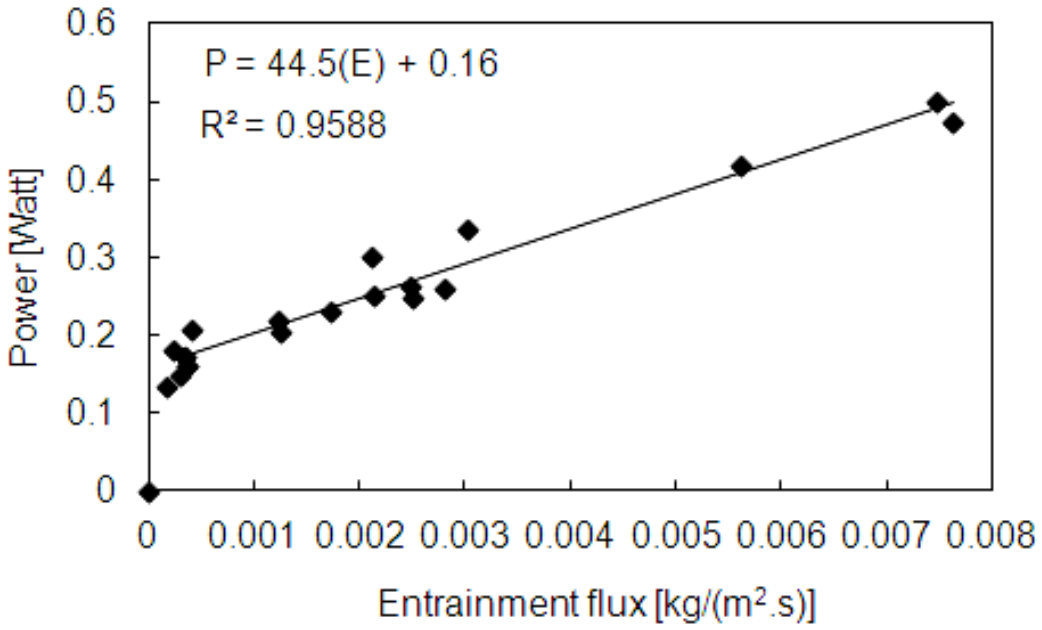

Figure 13: Calibration curve for the solid mass flow meter.

The fitted line does not go through the origin. This implies that there is some other effect causing the flow meter plate to require a higher power input per mass of solids flow. At low entrainment fluxes (< 3.4 x 10^{-4} kg/(m^2.s)) the fine particles have a high residence time on the mass flow meter due to low shear forces resulting in more heat transfer between the fine particles and the flow meter

resulting in a relatively high power requirement for a very low solids flow rate. As the entrainment flux increases beyond 3.4 x 10^{-4} kg/(m^2.s) the shear forces and interparticle collisions increase resulting in a decrease in the residence time of the solids.

At high entrainment fluxes (> 7.5 x 10^{-3} kg/(m^2.s)), the calibration curve predictions are unreliable due to the significant variation in the temperature of the mass flow meter plate as discussed in Section 4.2.3.

Different entrainment values were obtained for the same air velocity. This can be explained by the fact that fines that are not separated from the gas by the cyclones and collected in the filter bags were not returned to the bed after each experiment. The powder in the filter bags were returned to the bed only when the filter bags are full. However, the entrainment values as a function of power requirement by the measurement plate still follow the linear calibration curve in Figure 13.

4.5 Comparison with the measurement device developed by De Vos and co-workers (2010)

The calibration curve for the entrainment measurement device developed by De Vos and co-workers (2010) is given in Figure 14. From the shape of the calibration curve, it can be seen that the sensitivity of the flow meter decreases as the entrainment increases. A linear relationship was obtained for the calibration curve developed in this investigation (Figure 13) up to a maximum entrainment flux of 7.5 x 10^{-3} kg/(m^2.s). It may be possible to extend the linear region beyond 7.5 x 10^{-3} kg/(m^2.s) when a more accurate controller is used.

In order to determine the linear section of the calibration curve of the mass flow meter developed by De Vos and co-workers (2010) a line was fitted through the calibration data points in Figure 14. The best linear fit that could be obtained was used (R^2 value as close as possible to the R^2 value obtained for the data given in

Figure 13). The turndown ratio of this linear section shown in Figure 14 is approximately 7. Using the calibration data given in Figure 13, the turndown ratio of the linear section of the curve was calculated as 22. The mass flow meter developed in this investigation can therefore be used over a wider range of entrainment rates.

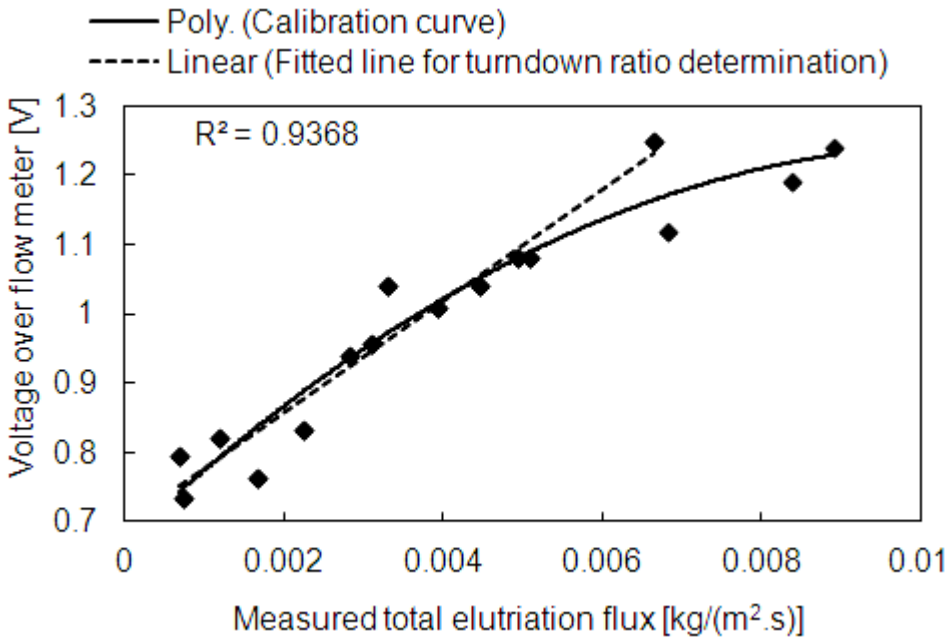

Figure 14: Calibration curve (taken from De Vos *et al*, 2010).

5. Case study

Briens and co-workers (1992) found that the flux of entrained particles increases when charge is neutralised or reduced in the fluidization column. According to Wang and co-workers (2009) charge can be successfully eliminated by introducing chemical static agents e.g. ethanol to the column. Adding ethanol to the inlet air supply of the fluidization column could therefore result in measurable changes in the entrainment rate without a significant change in the gas superficial velocity. In order to test the ability of the mass flow meter to detect these changes during continuous operation, ethanol was subsequently dosed to the inlet air supply of the fluidization column.

To operate continuously the shut-off disc below the solid mass flow meter was removed; therefore no solids collection took place. Ethanol (96 %) at 40 °C was dosed using two methods. In the first method ethanol was injected with a 20 ml syringe into the air feed stream and in the second method ethanol was continuously injected through a 0.3 mm hole into the air feed stream using a Heidolph 5201 peristaltic pump. The air velocity was kept constant at 0.26 m/s for both the batch and continuous ethanol dosing experiments.

5.1 Batch dosing

The syringe dosing experiments were conducted before the rainy season; when the humidity of the air was between 11 % and 12 %. Two experiments were conducted. In the first experiment 20 ml of ethanol was injected with a syringe into the air feed stream over a period of two minutes. The response curve obtained is given in Figure 15. An increase can be seen in the entrainment when ethanol was injected. After ethanol injection the higher entrainment was maintained for a short while, before the entrainment started decreasing back to the steady state obtained during fluidization before ethanol was injected.

In the second experiment 20 ml of ethanol was injected twice. Each injection

lasted one minute and the second injection was done directly after the first injection. After ethanol injection the entrainment increased twice forming two peaks in the response curve before returning back to the original steady state as shown in Figure 16. The two distinct peaks observed in Figure 16 is most likely a result of the discontinuity in the injection of the ethanol.

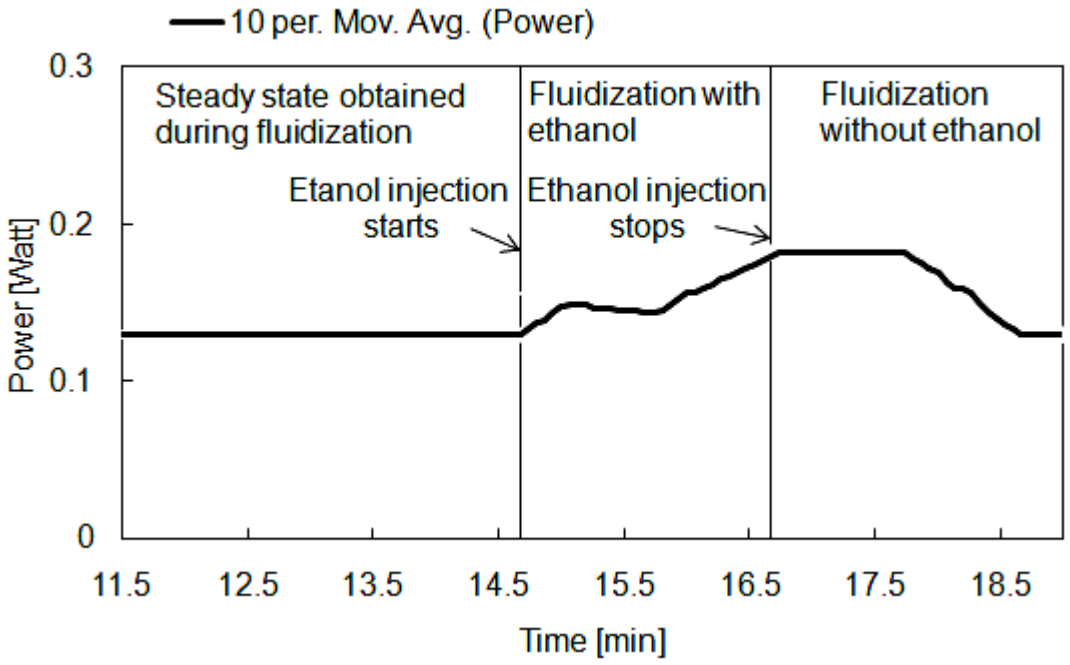

Figure 15: Effect of ethanol on entrainment at an ethanol injection rate of 10 ml/min.

In the second experiment 20 ml of ethanol was injected twice. Each injection

The reason for the increase in entrainment with the injection of ethanol may be that the ethanol has a neutralizing effect on the electrostatic charges. Subsequently fewer particles are attached to the wall of the column and to other particles. The particles can move more freely resulting in an increase in entrainment.

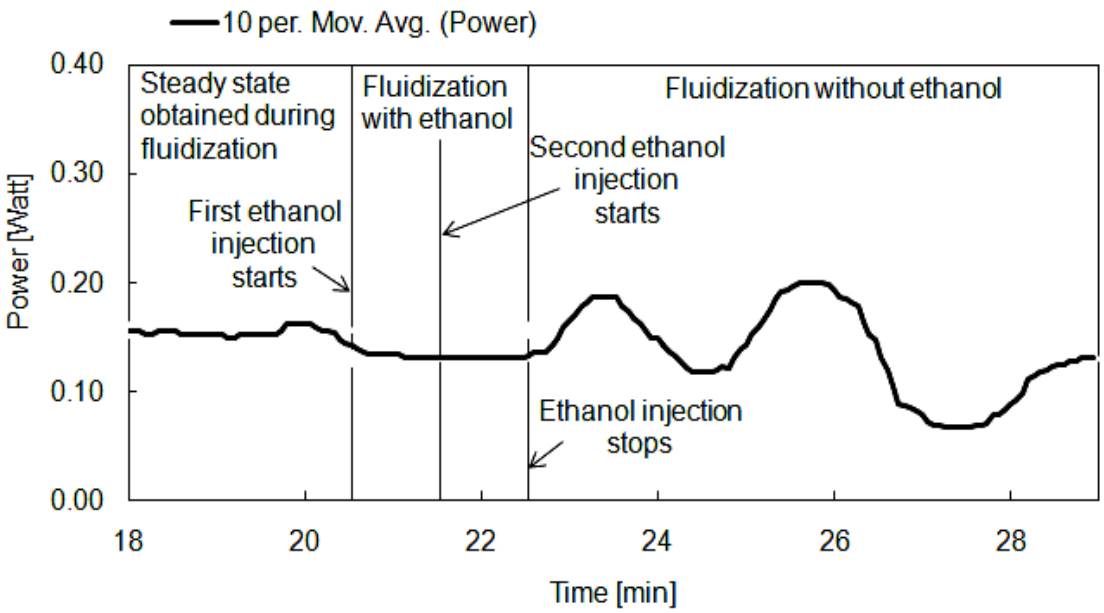

Figure 16: Effect of ethanol on entrainment at an ethanol injection rate of 20 ml/min.

5.2 Continuous dosing

The continuous dosing experiments were conducted during the rainy season; when the humidity of the air was between 38 % and 40 %. The steady state obtained during fluidization before ethanol injection is approximately the same for the batch dosing and continuous dosing experiments (see Figures 15-20); even though the air humidity was different. Concluding that the air humidity had an insignificant effect on the entrainment rate.

The ethanol injection rates that were investigated are: 10 ml/min, 20 ml/min, 30 ml/min and 40 ml/min. Injecting ethanol at a rate of 10 ml/min caused the entrainment to increase as shown in Figure 17. An injection rate beyond 10 ml/min caused the entrainment to decrease. The decrease in entrainment at injection rates of 30 ml/min and 40 ml/min was greater compared to an injection rate of 20 ml/min as can be seen in Figures 18 to 20.

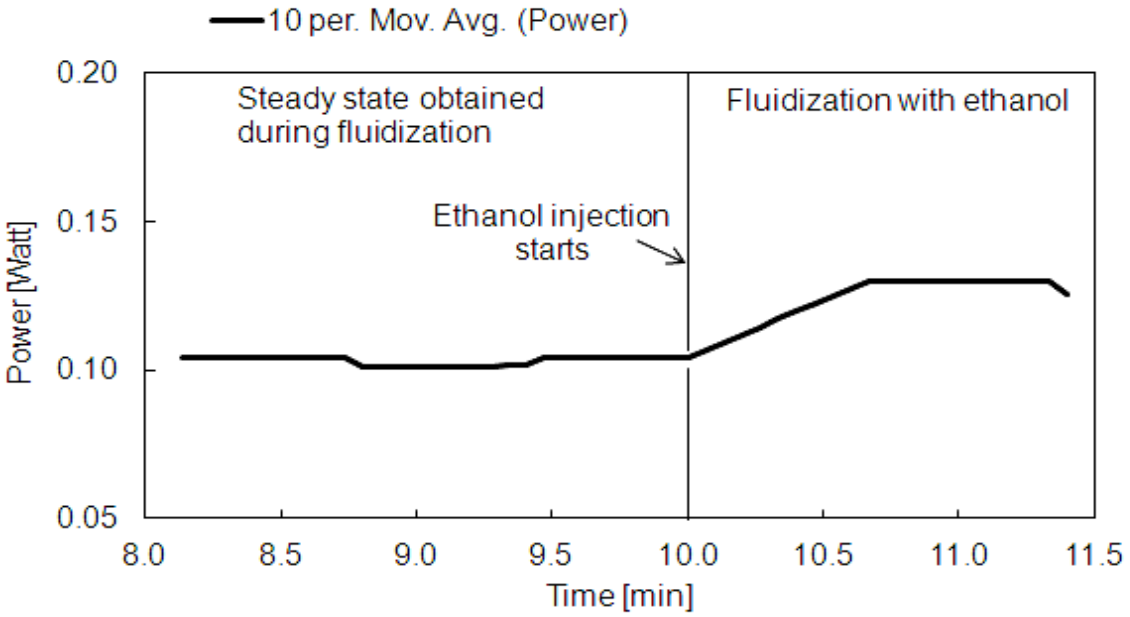

Figure 17: Effect of ethanol on entrainment at an ethanol feed rate of 10 ml/min.

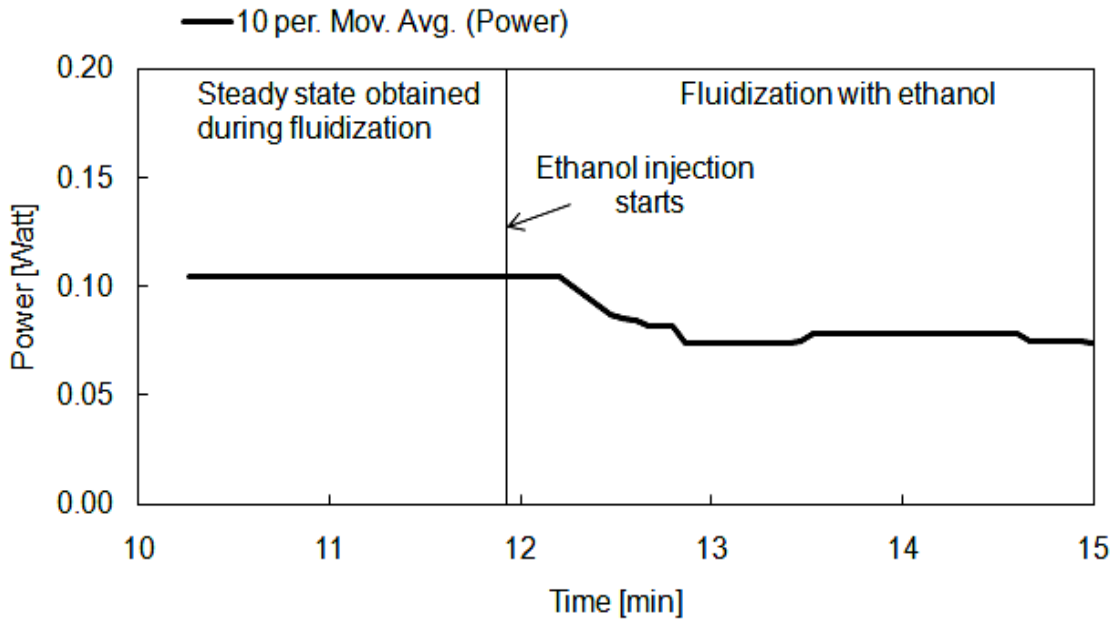

Figure 18: Effect of ethanol on entrainment at an ethanol feed rate of 20 ml/min.

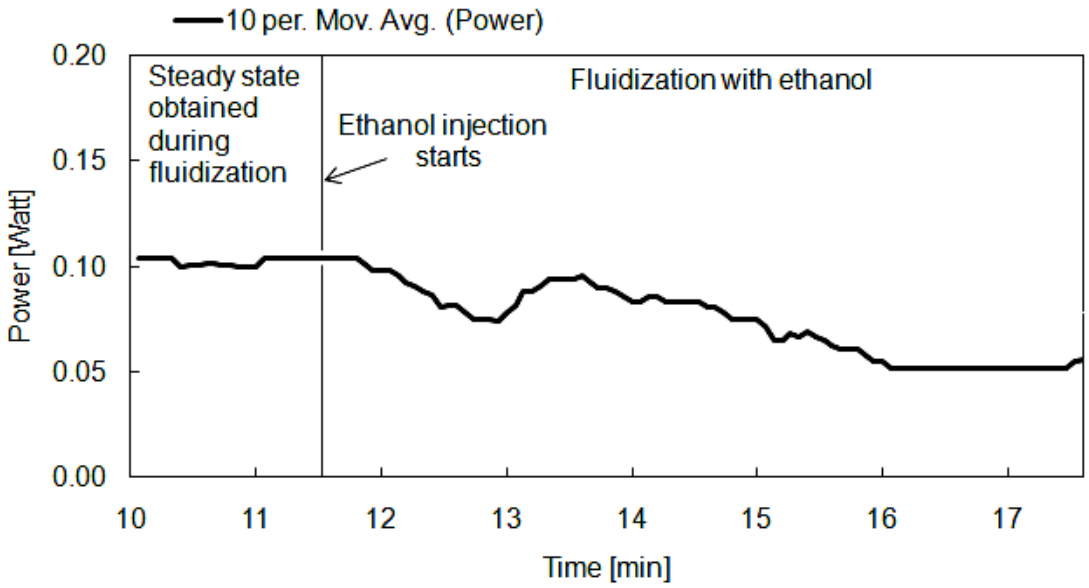

Figure 19: Effect of ethanol on entrainment at an ethanol feed rate of 30 ml/min.

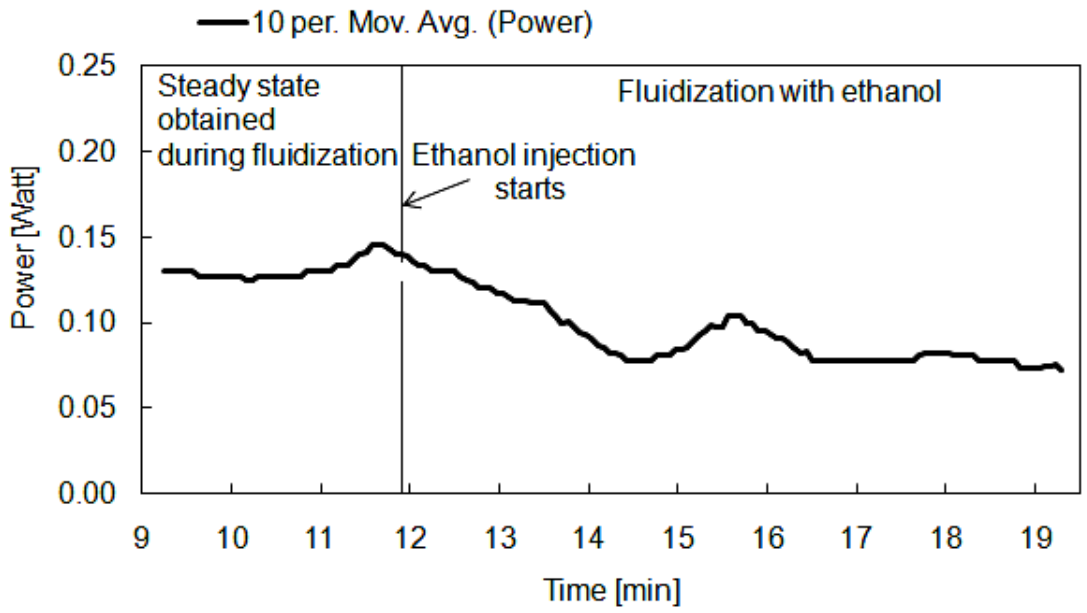

Figure 20: Effect of ethanol on entrainment at an ethanol feed rate of 40 ml/min.

The increase in entrainment observed at the lower ethanol dose, can also be explained by the electrostatic charge neutralizing effect discussed in Section 5.1. This result is similar to the findings of Wang and co-workers (2009) who found

that charge can successfully be eliminated by adding a chemical static agent like ethanol to the air feed stream (as discussed in Section 2.2.2).

The difference in the response curves obtained at the same injection rate of 20 ml/min between the batch dosing (Figure 16) and continuous dosing (Figure 18) experiments may be due to the different techniques used to inject the ethanol as well as the overall duration of ethanol dosing. With the batch dosing experiments there was a discontinuity between the two subsequent 20 ml injections, while the ethanol was dosed continuously at this rate over a time period of three minutes for the continuous dosing experiments.

The reason for the subsequent decrease in entrainment rate at higher ethanol dosing rates is ascribed to an increase in the cohesivity of the bed. The liquid droplets of ethanol in the air made the bed behave cohesively. A decrease in entrainment was also observed by Geldart and Wong (1985) (quoted by Briens *et al* (1992)) as discussed in Section 2.2.2. Geldart and Wong (1985) related the decrease in entrainment rate to an increase in powder cohesivity with relative humidity.

The results from the case study indicate that the flow meter can be used to detect changes in entrainment rate online during continuous operation.

6. Conclusions

A solid mass flow meter was developed that uses the principles of a thermal mass flow meter and constant temperature anemometry. The mass flow meter consisted of a measurement plate with eight resistors which were connected in series. An electrical current was sent through the resistors in order to heat the plate. A fixed temperature difference of 7 ºC was maintained between the plate and the environment. Two temperature sensors attached to the bottom of the plate were used to measure the plate temperature and the temperature was controlled by modulating the power to the resistors using pulse width modulation.

Due to conductive heat transfer between the entrained solids and the measurement plate, additional power was needed to maintain the setpoint temperature. This additional power was correlated against the average solids flow rate. The mass flow meter was able to measure the total entrainment flux in the range of 1.7×10^{-4} kg/(m^2.s) to 7.5×10^{-3} kg/(m^2.s).

The calibration curve was corrected for the power needed to keep the plate at the setpoint temperature and for the heat gained or lost to the environment. A 30 % to 39 % contribution was made to the power measurements by the turbulence in the dipleg caused by the air vortex effect from the exits of the cyclones.

The calibration curve shows a linear relationship between the power measurement and the entrainment flux for entrainment fluxes between 3.4×10^{-4} kg/(m^2.s) and 7.5×10^{-3} kg/(m^2.s). At lower entrainment fluxes the fine particles have a high residence time on the measurement plate due to low shear forces resulting in more heat transfer between the fine particles and the measurement plate and therefore a higher power requirement for a very low solids flow rate. At higher entrainment fluxes the power measurements were unreliable due to poor temperature control.

The mass flow meter maintains its sensitivity over the investigated entrainment range and the turndown ratio of the linear part of the calibration curve is approximately three times that of the mass flow meter developed by De Vos and co-workers (2010).

In order to test the ability of the mass flow meter to detect changes in entrainment rate during continuous operation with no change in superficial gas velocity, ethanol was dosed to the inlet air supply of the fluidization column using a syringe (batch) or continuously dosed using a peristaltic pump.

An increase in the entrainment rate was obtained when ethanol was dosed at a rate of 10 ml/min, but at dosing rates beyond 10 ml/min the entrainment rate decreased. The increase and decrease were ascribed to a reduction in the static electricity of the bed and an increase in the powder cohesivity of the bed respectively. The results from the case study indicate the suitability of the flow meter to detect changes in entrainment rate online during continuous operation.

7. Recommendations

- A controller that provides more accurate and stable control should be used in order to minimize the overshoot in the power response curves and to minimize the variation in the temperature response obtained at high entrainment rates.

- The controller should be programmed to use a shorter sampling interval so that the entire power response curve can be followed.

- Entrainment experiments should be conducted at low entrainment fluxes ($< 3.4 \times 10^{-4}$ kg/(m^2.s)) by using a stronger vibrating or similar device against the dipleg. The vibrating device is used to overcome the attraction forces between the fine particles and the mass flow meter plate; thereby reducing the residence time of the fine particles. These experiments can be used to confirm whether the calibration curve goes through the origin if the attraction forces are overcome.

- The ethanol experiments should be repeated by adding ethanol vapour to the air feed stream, thereby preventing the liquid from accumulating at the bottom of the pipeline before being carried into the bed by the passing air. The ethanol experiments should also be repeated using air with a constant humidity in order to compare the results from the continuous injection and batch injection more accurately.

- The electrostatic charge of the bed should be measured before and after ethanol injection into the air feed stream to determine if the increase in entrainment that was observed was due to a reduction in the electrostatic charge of the bed.

8. References

- Almendros-Ibáñez, JA, Sánchez-Delgado, S, Sobrino, C and Santana, D (2009) “Experimental observations on the different mechanisms for solid ejection in gas-fluidized beds”, *Chemical Engineering and Processing*, *48*, 734-744.

- Baeyens, J, Geldart, D and Wu, SY (1992) “Elutriation of fines from gas fluidized beds of Geldart A-type powders – effect of adding superfines”, *Powder Technology*, *71*, 71 – 80.

- Baron, T, Briens, CL, Galtier, P and Bergougnou, MA (1990) “Effect of bed height on particle entrainment from gas-fluidized beds”, *Powder Technology*, *63*, 149 – 156.

- Bhusarapu, S, Al-Dahhan, M and Dudukovic, MP (2004a) “Quantification of solids flow in a gas-solid riser: single radioactive particle tracking”, *Chemical Engineering Science*, *59*, 5381-5386.

- Bhusarapu, S, Fongarland, P, Al-Dahhan, MH and Duduković, MP (2004b) ”Measurement of overall solids mass flux in a gas-solid circulating fluidized bed”, *Powder Technology*, *148*, 158-171.

- Blastrite (2011) “Technical Product Information”, Blastrite, Industrial Minerals, Germiston.

- Boland, D and Geldart, D (1971) “Electrostatic charging in gas fluidised beds”, *Powder Technology*, *5*, 289-297.

- Briens, CL, Bergougnou, MA, Inculet, II, Baron, T and Hazlett, JD (1992) “Size distribution of particles entrained from fluidized beds: electrostatic

effects", *Powder Technology*, *70*, 57 – 62.

- Choi, J-H, Chang, I-Y, Shun, D-W, Yi, C-K, Son, J-E and Kim, S-D (1999) "Correlation on the particle entrainment rate in gas fluidized beds", *Ind. Eng. Chem. Res.*, *38* (6), 2491-2496.

- Cilliers, D (2011) "Pulse width modulation", Personal Communication, Colibritec Technologies.

- De Vos, WP, Du Toit, EL and Nicol, W (2010) "Dynamic elutriation measurement in a continuously operated bubbling fluidized bed", *Fluidization XIII, New Paradigm in Fluidization Engineering*, Engineering Conferences International, 129-135.

- De Vos, W, Nicol, W and Du Toit, E (2009) "Entrainment behaviour of high-density Geldart A powders with different shapes", *Powder Technology*, *190*, 297 – 303.

- Do, HT, Grace, JR and Clift, R (1972) "Particle ejection and entrainment from fluidised beds", *Powder Technology*, *6*, 195 - 200.

- Fung, AS and Hamdullahpur, F (1993) "Effect of bubble coalescence on entrainment in gas fluidized beds", *Powder Technology*, *77*, 251-265.

- Greeff, IL and Skinner, W (2000) *Piping System Design*, Department of Chemical Engineering, University of Pretoria.

- Han, Y-L, Chyang, C-S, Hsiao, W-M and Lo, K-C (2011) "Effects of fines hold-up in the freeboard on elutriation from a fluidized bed", *Journal of the Taiwan Institute of Chemical Engineers*, *42*, 120 – 123.

- Harris, BJ, Davies, CE and Davidson, JF (1997) “The slot flow meter: a new device for continuous solids flow measurement”, *Chemical Engineering Science*, *52*, 4637-4648.

- Hatano, M and Ishida, M (1983) “Study on the entrainment of FCC particles from a fluidized bed”, *Powder Technology*, *35*, 201-209.

- In-Flow (*sa*) “Industrial Style Digital Mass Flow Meters and Controllers for Gases”, Bronkhorst High Tech.

- Kunii, D and Levenspiel, O (1990) “Entrainment of solids from fluidized beds I. Hold-up of solids in the freeboard II. Operation of fast fluidized beds”, *Powder Technology*, *61*, 193-206.

- Kunii, D and Levenspiel, O (1991) *Fluidization Engineering*, Butterworth-Heinemann, USA.

- Liu, Z, Takafuji, M and Suda, T (2011) “The effect of riser scale on the hydrodynamics and particle residence-time distribution”, paper presented at *Industrial Fluidization South Africa*, 16 – 17 November, 2011, Johannesburg, South Africa, 257-266.

- Lötters, J (1999) “Economical thermal mass flow sensor based on constant temperature anemometry”, paper presented at *Sensor 99*, Nűrnberg, Germany.

- MSDS (2003) “Material Safety Data Sheet”, Starbead® Industrial Beads, Blastrite.

- National Semiconductor (2000) “LM35 Precision Centigrade Temperature Sensors”, National Semiconductor Corporation.

- Nicol, W (2011) “Shortcomings of the on-line solid mass flow meter”, Personal Communication, Department of Chemical Engineering, University of Pretoria.

- Park, A-H, Bi, H and Grace, JR (2002) “Reduction of electrostatic charges in gas-solid fluidized beds”, *Chemical Engineering Science*, *57*, 153-162.

- Parr (2012) “Fluidized bed reactors”, Parr Instrument Company, www.parrinst.com/products/specialty-custom.../fluidized-bed-reactors/?pdf [2012, February 8].

- Rhodes, M (1998) *Introduction to Particle Technology,* John Wiley & Sons, England.

- Sensirion (2010) “Datasheet SHT7x (SHT71, SHT75), Humidity and Temperature Sensor”, The Sensor Company, Sensirion.

- Sinnot, RK (2005) *Chemical Engineering Design*, Volume 6, Elsevier Butterworth-Heinemann, Oxford.

- Spenik, JL and Ludlow, JC (2010) “Use of piezoelectric pressure transducers to determine local solids mass flux in the riser of a cold flow circulating bed”, *Powder Technology*, *203*, 86-90.

- Wang, J, Xu, Y, Li, W, Yang, Y and Wang, F (2009) “Electrostatic potentials in gas-solid fluidized beds influenced by the injection of charge inducing agents”, *Journal of Electrostatics*, *67*, 815-826.

- Yang, W, (2003) *Handbook of Fluidization and Fluid-Particle Systems*, Marcel Dekker, Inc., New York.

- Zheng, Y and Liu, Q (2011) “Review of techniques for the mass flow rate measurement of pneumatically conveyed solids”, *Measurement*, *44*, 589-604.